WAVE PROPAGATION IN LOSSY WAVEGUIDE STRUCTURES

by

Steven E. Bucca

Thesis submitted to the Faculty of the
Virginia Polytechnic Institute and State University
in partial fulfillment of the requirements for the degree of

MASTER OF SCIENCE

in

Electrical Engineering

APPROVED:

William A. Davis, Chairman

Sedki M. Riad

Gary S. Brown

December, 1989

Blacksburg, Virginia

WAVE PROPAGATION IN LOSSY WAVEGUIDE STRUCTURES

by

Steven E. Bucca

Dr. William A. Davis, Chairman

Electrical Engineering

(ABSTRACT)

In this thesis a numerical technique is developed determining the propagation constant in waveguides and transmission lines. The technique accounts for both dielectric and conductor losses in a guide having an arbitrary cross section and uses a full-wave solution process. A set of coupled, vector integral equations which characterize the system are derived. The equations enforce the necessary boundary conditions on the tangential electric and magnetic fields at the boundaries separating the conductors and dielectrics.

The method of moments (MOM) technique is used to cast the equations into a numerically solvable form. Computed results for various waveguide structures are compared to known or perturbed results for three well-known structures. However, the program is more general and may be applied to other cross-sections. Finally, possible future extensions of the work is presented.

Acknowledgements

I take this opportunity to acknowledge all those who have guided, supported, and struggled with me during the completion of this thesis. I especially wish to thank my wife whose love and support have given me much needed encouragement. I also extend specific thanks to whose guidance and patience has contributed greatly to the completion of this thesis. I am also grateful to the other members of my committee, Dr. Gary S. Brown and Dr. Sedki M. Riad. Finally, I wish to recognize the E. I. Dupont Corporation and the Center for Innovative Technology for their support.

Table of Contents

Chapter 1

Introduction

Wave propagation in microwave guiding structures has long been a subject of interest. Since the advent of the digital computer, the propagation effects due to cross–sectional geometry and material properties have been widely studied. The computer has allowed the study of waveguides having unusual cross-sections, multi-layered dielectrics, and multi-conductor paths. However, the effects of non-ideal conductors is an area that has not received such widespread attention.

The most important effect of non-ideal conductors is signal loss. To quantify the loss, most researchers have used a perturbation approach [1,73]. With this approach the fields and propagation constant are first determined for the lossless case and the loss is then approximated by using the lossless fields at the conducting surfaces. Naturally, this technique is limited to low-loss situations. In addition to creating loss, non-ideal conductors also modify the phase of the signal. With the perturbation approach described above, this effect is completely ignored. To fully account for the conductor effects, a more complete analysis is needed.

The analysis developed in this thesis determines the propagation constant in microwave guiding structures. The resulting technique, a full-field analysis, allows the structure to have a general cross-section and accounts for both conductor and dielectric loss. The full-field analysis uses the vector potential representations of the fields and the equivalence principle [1,106] to express the fields as integrals over the media boundaries in the structure (e.g. the

dielectric/conductor boundary). A set of coupled integral equations, which may be solved for the structure'propagation constant, is obtained by matching the field components across these boundaries. These integral equations are solved by using a popular numerical technique — the method of moments (MOM). The MOM technique reduces the set of coupled integral equations to a set of simultaneous linear equations, which may be solved by a number of well-known techniques (e.g. LU decomposition — lower/upper triangularization).

The remainder of this thesis is divided into five chapters and three appendicies. Chapter 2 develops the vector potential representations of electromagnetic fields. Chapter 3 derives the coupled integral equations for both waveguides and coaxial transmission lines, with special emphasis given to the waveguide problem. In chapter 4 the integral equations for the waveguide problem equations are cast into a numerically solvable form, and chapter 5 presents computer derived results for several waveguide structures. Chapter 6 summarizes the main topics of the thesis and discusses the primary conclusions. The three appendicies contain details of the derivations in chapters four and five.

Chapter 2

Preliminary Topics: Vector Potential Representation of Electromagnetic Fields

2.1 Introduction

In this chapter we "lay the groundwork" for the upcoming analytical development. The vector potential representations of electromagentic fields are presented, with a special emphasis on two-dimensional fields. In addition, terminology, definitions, and coordinate systems are introduced.

2.2 Vector Potential Representations of Two-Dimensional Electromagnetic Fields in a Homogeneous and Isotropic Region

Consider a homogeneous isotropic media characterized by a complex permittivity ϵ^* and complex permeability μ^*. Furthermore, let electric currents J and magnetic currents M exist in the region. From the results of Appendix A, the electromagnetic fields may be expressed in terms of the magnetic vector potential A and electric vector potential F as

$$\mathbf{E}(\mathbf{r}) = -\nabla \times \mathbf{F}(\mathbf{r}) + \frac{1}{j\omega\epsilon^*}\left(\nabla\left(\nabla \cdot \mathbf{A}(\mathbf{r})\right) + k^2\,\mathbf{A}(\mathbf{r})\right) \tag{2.1}$$

$$\mathbf{H}(\mathbf{r}) = \nabla \times \mathbf{A}(\mathbf{r}) + \frac{1}{j\omega\mu^*}\left(\nabla\left(\nabla \cdot \mathbf{F}(\mathbf{r})\right) + k^2\,\mathbf{F}(\mathbf{r})\right), \tag{2.2}$$

with

$$\nabla^2 \mathbf{A}(\mathbf{r}) + k^2 \mathbf{A}(\mathbf{r}) = -\mathbf{J}(\mathbf{r}) \tag{2.3}$$

$$\nabla^2 \mathbf{F}(\mathbf{r}) + k^2 \mathbf{F}(\mathbf{r}) = -\mathbf{M}(\mathbf{r}) \tag{2.4}$$

where $\mathbf{r}$ is the 3-dimensional position vector locating a point in space and $k^2 \equiv \omega^2 \mu^* \epsilon^*$.

The del operator ∇ may be conveniently defined as

$$\nabla = \nabla_{tr} + \hat{\mathbf{z}} \frac{\partial}{\partial z} \tag{2.5}$$

where ∇_{tr} is the two-dimensional (transverse to $\hat{\mathbf{z}}$) operator. We now consider solutions to equations (2.1) through (2.4) which exhibit wave propagation in the $\hat{\mathbf{z}}$ direction (two-dimensional solutions). Specifically, we desire solutions where the z variation in all quantities is given by $e^{-jk_z z}$,

$$\mathbf{E}(\mathbf{r}) = \mathbf{E}(\rho)\, e^{-jk_z z} \quad , \quad \mathbf{H}(\mathbf{r}) = \mathbf{H}(\rho)\, e^{-jk_z z} \tag{2.6a}$$

$$\mathbf{J}(\mathbf{r}) = \mathbf{J}(\rho)\, e^{-jk_z z} \quad , \quad \mathbf{M}(\mathbf{r}) = \mathbf{M}(\rho)\, e^{-jk_z z} \tag{2.6b}$$

$$\mathbf{A}(\mathbf{r}) = \mathbf{A}(\rho)\, e^{-jk_z z} \quad , \quad \mathbf{F}(\mathbf{r}) = \mathbf{F}(\rho)\, e^{-jk_z z} \tag{2.6c}$$

where ρ represents the transverse to $\hat{\mathbf{z}}$ component of the position vector $\mathbf{r}$. The geometry dependent parameter k_z is an unknown quantity which must be determined. Only the values of k_z which satisfy Maxwell's equations and the boundary conditions are valid; the purpose of this thesis is to find the allowed k_z values for waveguide and transmission line problems.

The electric field $\mathbf{E}(\rho)$ may be expressed in terms of a $\hat{\mathbf{z}}$ component and transverse components as $\mathbf{E}(\rho) = \mathbf{E}_{tr} + E_z \hat{\mathbf{z}}$ (unless explicitly denoted otherwise, the implied argument ρ will be dropped in the text that follows). If we substitute (2.6) into (2.1) through (2.5) and perform some elementary vector manipulations, we obtain

$$E_z = -\left(\nabla_{tr} \times \mathbf{F}_{tr}\right) \cdot \hat{\mathbf{z}} + \frac{1}{j\omega\epsilon^*}\left(\left(k^2 - {k_z}^2\right) A_z - jk_z \left(\nabla_{tr} \cdot \mathbf{A}_{tr}\right)\right) \tag{2.7a}$$

and

$$\mathbf{E}_{tr} = jk_z \hat{\mathbf{z}} \times \mathbf{F}_{tr} - \nabla_{tr} F_z \times \hat{\mathbf{z}} +$$

$$\frac{1}{j\omega\epsilon^*}\left(\nabla_{tr}\left(\nabla_{tr} \cdot \mathbf{A}_{tr}\right) - jk_z \nabla_{tr} A_z + k^2 \mathbf{A}_{tr}\right), \tag{2.7b}$$

with

$$\nabla_{tr}^2 \mathbf{A}(\rho) + (k^2 - k_z{}^2)\mathbf{A}(\rho) = -\mathbf{J}(\rho) \tag{2.8}$$

$$\nabla_{tr}^2 \mathbf{F}(\rho) + (k^2 - k_z{}^2)\mathbf{F}(\rho) = -\mathbf{M}(\rho). \tag{2.9}$$

The equations for the magnetic field $\mathbf{H}(\rho)$ are similar to (2.7) and may be obtained via duality [1,98].

2.3 Helmholtz Integral Solutions for Two-Dimensional Electromagnetic Fields

Suppose we have two-dimesional sources acting in a homogeneous, isotropic, and unbounded media (Fig. 2.1). The source coordinates are denoted by ρ' and the field coordinates by ρ. The surface S denotes the area over which the sources act. For this case possible solutions to (2.8) and (2.9) are given by the two-dimesional Helmholtz integrals [1,228]

$$\mathbf{A}(\rho) = \frac{1}{j4}\iint_S \mathbf{J}(\rho')\, H_o^{(2)}(k_\rho |\rho - \rho'|)\, ds' \tag{2.10}$$

$$\mathbf{F}(\rho) = \frac{1}{j4}\iint_S \mathbf{M}(\rho')\, H_o^{(2)}(k_\rho |\rho - \rho'|)\, ds' , \tag{2.11}$$

where

$H_o^{(2)}(\cdot)$ is the zeroth order Hankel function of the second kind

$k_\rho \equiv \sqrt{k^2 - k_z{}^2}$

ds' is an element of area perpendicular to z.

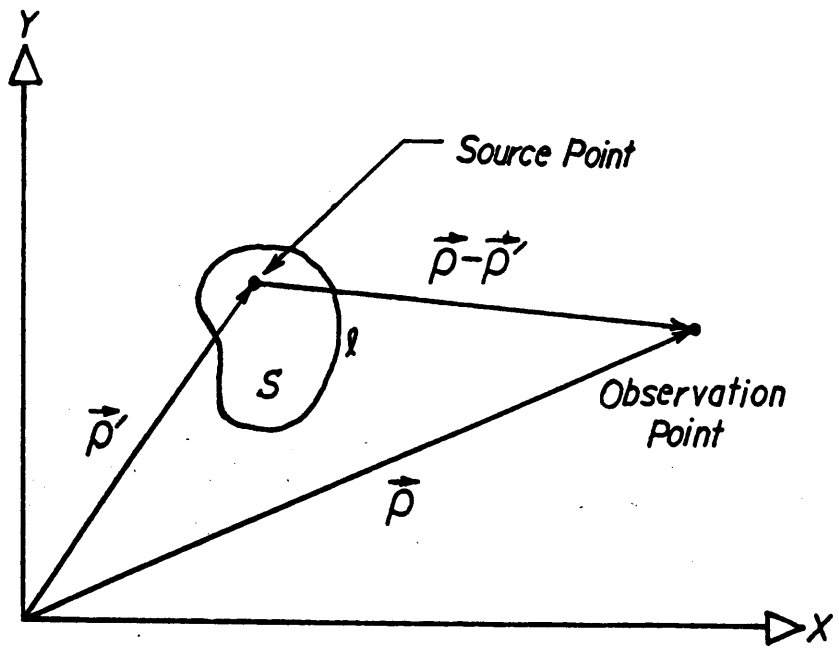

Figure 2.1. Coordinate system for 2-Dimensional field problems.

For the case where only surface currents exist on the boundary of the surface S (denoted by the contour ℓ – Fig. 2.1) then (2.10) and (2.11) become

$$\mathbf{A}(\rho) = \frac{1}{j4} \oint_{\ell} \mathbf{J}(\rho')\, H_o^{(2)}(k_\rho |\rho - \rho'|)\, d\ell' \tag{2.12}$$

$$\mathbf{F}(\rho) = \frac{1}{j4} \oint_{\ell} \mathbf{M}(\rho')\, H_o^{(2)}(k_\rho |\rho - \rho'|)\, d\ell' \tag{2.13}$$

where $d\ell'$ is an elemental length of the contour ℓ and $\oint$ represents an integral over the closed contour ℓ.

Chapter 3

Analytical Development

3.1 Integral Representations of the Electric Field via the Equivalence Principle

Consider the infinitely long (no variation with respect to z) source-free waveguide shown in Fig. 3.1. Both the conductor and dielectric regions are assumed to be isotropic and homogeneous. The dielectric, characterized by a complex permittivity ϵ_d^* and permeability μ_d^*, supports the fields $(\mathbf{E}^d,\mathbf{H}^d)$, while the conductor contains the fields $(\mathbf{E}^c,\mathbf{H}^c)$ and is characterized by an equivalent permittivity ϵ_c^*[1] and permeability μ_c^*. To simplify the development we will model the conductor as being infinitely thick. The model imposes no serious limitations provided the actual conductor is at least several skin depths thick (this is case in most practical metallic walled guides) [1,53] .

To formulate the problem the equivalence principle [1,106] is used. We shall find that the fields in the dielectric and/or the conductor regions may be expressed in terms of Helmholtz integrals with equivalent sources on the interface between the two media. The required integral equations are then obtained by matching the field components at the interface. In the

---

[1]Typically, conductors are characterized by a finite conductivity. The definition of ϵ_c^* implicitly includes the effects of the conductivity. For example, if the conductor has a conductivity σ and a permitivity ϵ_0, then the equivalent permitivity would be $\epsilon_c^* \equiv \epsilon_0\left(1 - j\frac{\sigma}{\omega\epsilon_0}\right)$.

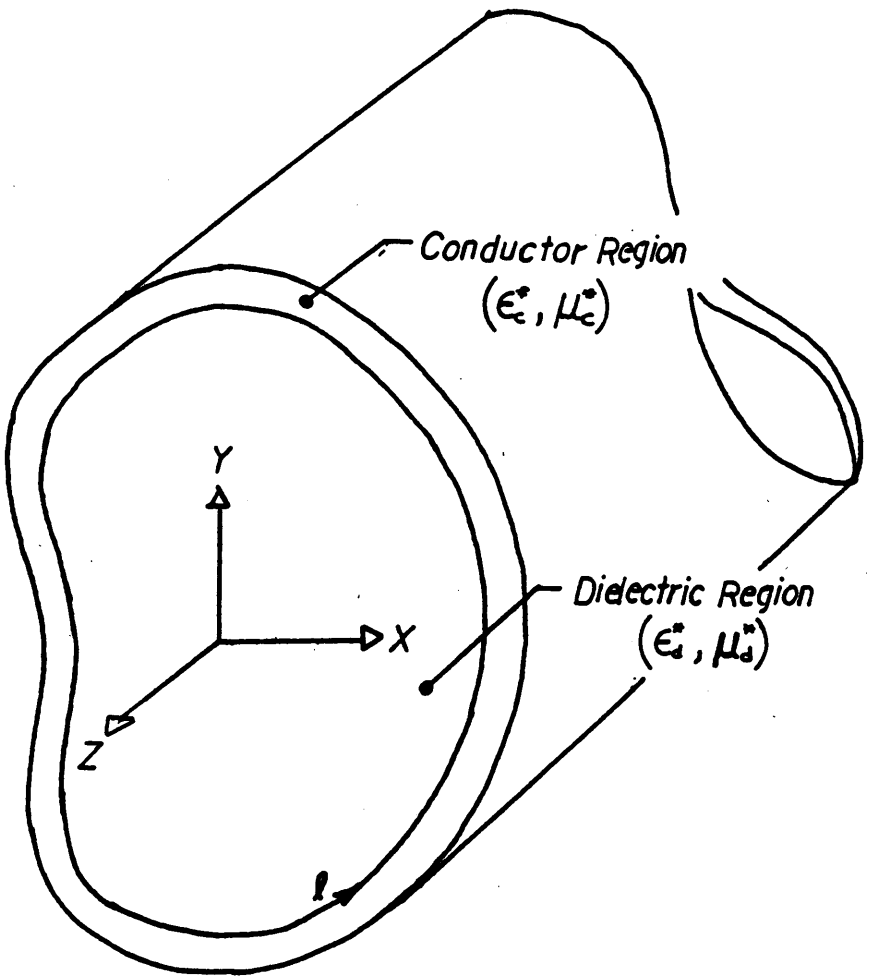

Figure 3.1. Cross-section of waveguide.

derivation that follows, we concentrate on the electric field in the dielectric region. Instead of repeating laborious derivations, we use the duality principle [1,98] and analogy to easily obtain the representations of all other fields.

The electric field in the dielectric region may be found using the following form of the equivalence principle (see Fig. 3.2). Internal to the boundary ℓ (in the dielectric region) we propose the original fields ($\mathbf{E}^{\mathrm{d}}$,$\mathbf{H}^{\mathrm{d}}$), and external to ℓ (in the conductor region) we propose null fields (0,0). With this assumption, we may replace the conductor media by the dielectric media. To satisfy the boundary conditions [1,34], surface currents must exist on the boundary separting the two regions. If we seek two-dimensional solutions (z variation given by $e^{-jk_z z}$) then the equivalent surface currents are given by

$$\mathbf{J}^{\mathrm{d}} = +\hat{\mathbf{n}}' \times \mathbf{H}^{\mathrm{d}}\big|_{\ell} \tag{3.1}$$

$$\mathbf{M}^{\mathrm{d}} = -\hat{\mathbf{n}}' \times \mathbf{E}^{\mathrm{d}}\big|_{\ell} \tag{3.2}$$

where $\mathbf{E}^{\mathrm{d}}\big|_{\ell}$ and $\mathbf{H}^{\mathrm{d}}\big|_{\ell}$ represent the fields on the dielectric side of the boundary ℓ, and $\hat{\mathbf{n}}'$ represents the unit normal (to ℓ) directed into the dielectric region. The equivalent sources now act in a homogeneous, isotropic, and unbounded region — the conditions required to use the results of sections 2.2 and 2.3. Using the notation introduced with (2.7), the dielectric electric field ($\mathbf{E}^{\mathrm{d}}$) may now be expressed as

$$E_z^{\mathrm{d}} = -\left(\nabla_{tr} \times \mathbf{F}_{tr}\right) \cdot \hat{\mathbf{z}} + \frac{1}{j\omega\epsilon_{\mathrm{d}}^*}\left(\left(k_{\mathrm{d}}{}^2 - k_z{}^2\right)A_z - jk_z\left(\nabla_{tr} \cdot \mathbf{A}_{tr}\right)\right) \tag{3.3a}$$

and

$$\mathbf{E}_{tr}^{\mathrm{d}} = jk_z \hat{\mathbf{z}} \times \mathbf{F}_{tr} - \nabla_{tr} F_z \times \hat{\mathbf{z}}$$

$$+ \frac{1}{j\omega\epsilon_{\mathrm{d}}^*}\left(\nabla_{tr}\left(\nabla_{tr} \cdot \mathbf{A}_{tr}\right) - jk_z \nabla_{tr} A_z + k_{\mathrm{d}}{}^2 \mathbf{A}_{tr}\right), \tag{3.3b}$$

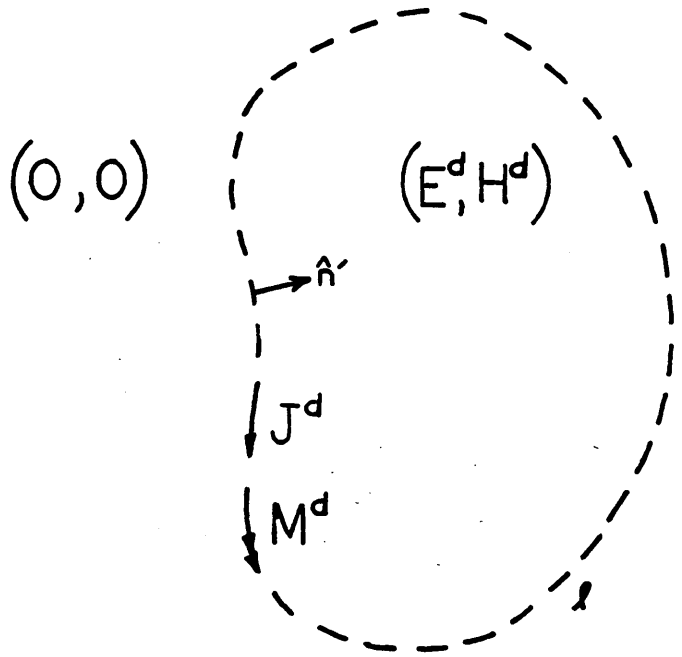

Figure 3.2. Equivalent problem for computing dielectric fields.

where

$$k_d^2 \equiv \omega^2 \mu_d^* \epsilon_d^* , \tag{3.4}$$

and

$$\mathbf{A} \equiv \mathbf{A}_{tr} + A_z \hat{\mathbf{z}} = \oint_\ell \mathbf{J}^d(\rho') \, G^d(\rho,\rho') \, d\ell' , \tag{3.5}$$

$$\mathbf{F} \equiv \mathbf{F}_{tr} + F_z \hat{\mathbf{z}} = \oint_\ell \mathbf{M}^d(\rho') \, G^d(\rho,\rho') \, d\ell' , \tag{3.6}$$

with

$$G^d(\rho,\rho') \equiv \frac{1}{j4} H_o^{(2)}(k_\rho^d |\rho-\rho'|), \tag{3.7}$$

$$k_\rho^d \equiv \sqrt{k_d^2 - k_z^2} . \tag{3.8}$$

Let us define two local coordinate systems (Fig. 3.3) — one at the observation point (located by ρ) and the other at the source location (located by ρ'). The coordinate system at the observation point has the ordered triple <n,t,z>, while the coordinate system at the source location has the ordered triple <n′,t′,z′>. For example, the electric field would be given by

$$\mathbf{E}^d \equiv \mathbf{E}_{tr}^d + E_z^d \hat{\mathbf{z}} \equiv E_t \hat{\mathbf{t}} + E_n \hat{\mathbf{n}} + E_z \hat{\mathbf{z}} \tag{3.9a}$$

and the electric current source by

$$\mathbf{J}^d \equiv \mathbf{J}_{tr}^d + J_z^d \hat{\mathbf{z}}' \equiv J_t \hat{\mathbf{t}}' + J_z \hat{\mathbf{z}}' \tag{3.9b}$$

(the absence of a normal component in 3.9b is a consequence of 3.1). We should also note that our particular choice of coordinates implies $d\ell' = dt'$. Equations (3.3a) and (3.3b) may now be expressed as (note $\hat{\mathbf{z}} = \hat{\mathbf{z}}'$)

$$E_z^d = -\left(\nabla_{tr} \times \oint_\ell G^d \, M_t \hat{\mathbf{t}}' \, dt' \right) \cdot \hat{\mathbf{z}} + \oint_\ell \frac{k_d^2 - k_z^2}{j\omega\epsilon_d^*} G^d \, J_z \, dt'$$

$$- jk_z \nabla_{tr} \cdot \oint_\ell \frac{1}{j\omega\epsilon_d^*} G^d \, J_t \hat{\mathbf{t}}' \, dt' \tag{3.10}$$

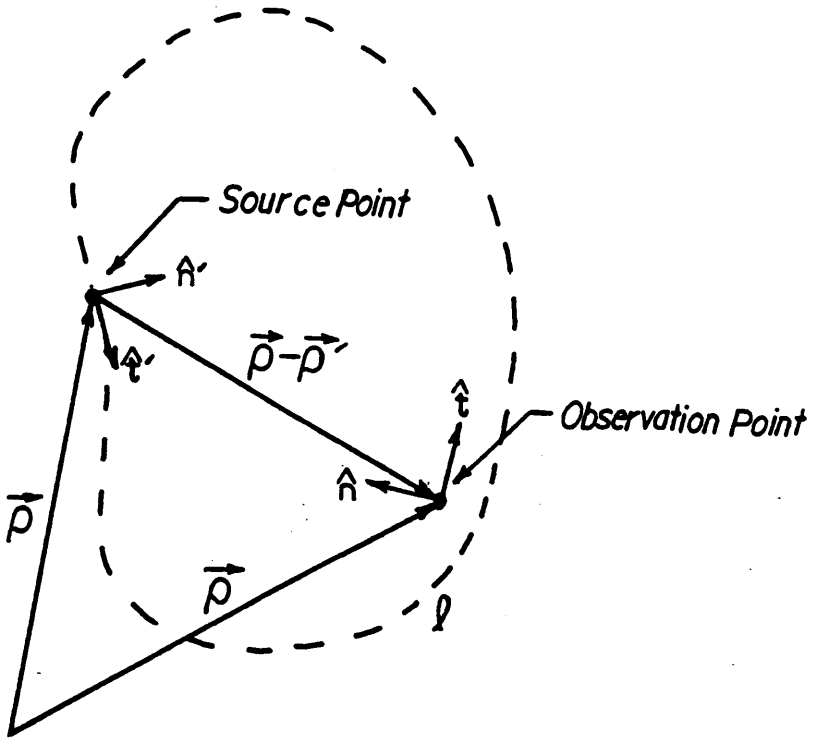

Figure 3.3. Local coordinate systems.

and

$$\mathrm{E}^{\mathrm{d}}_{tr} \equiv E^{\mathrm{d}}_t \hat{\mathbf{t}} + E^{\mathrm{d}}_n \hat{\mathbf{n}} = jk_z\,\hat{\mathbf{z}} \times \oint_\ell \mathrm{G}^{\mathrm{d}}\, M_t \hat{\mathbf{t}}'\, dt' + \hat{\mathbf{z}} \times \nabla_{tr} \oint_\ell \mathrm{G}^{\mathrm{d}}\, M_z\, dt'$$

$$+ \nabla_{tr}\left(\nabla_{tr} \cdot \oint_\ell \frac{1}{j\omega\epsilon^*_{\mathrm{d}}} \mathrm{G}^{\mathrm{d}}\, J_t \hat{\mathbf{t}}'\, dt' \right) - jk_z \nabla_{tr} \oint_\ell \frac{1}{j\omega\epsilon^*_{\mathrm{d}}} \mathrm{G}^{\mathrm{d}}\, J_z\, dt'$$

$$+ \oint_\ell \frac{k_{\mathrm{d}}^2}{j\omega\epsilon^*_{\mathrm{d}}} \mathrm{G}^{\mathrm{d}}\, J_t \hat{\mathbf{t}}'\, dt' \quad . \tag{3.11}$$

We shall later see that our devlopment will require that the fields be evaluated at the boundary ℓ, posing a "slight" complication. When the observation point is brought to the boundary, a point exists where the argument of the Green's function G^{d} will vanish (see Eqs. 3.5 – 3.7). At this point the Green's function contains a logarithmic singularity. For example, if we let $|\rho - \rho'| = \mathrm{P}$, then as $\mathrm{P} \to 0$ the Green's function behaves as [1,203]

$$\mathrm{G}(k_\rho \mathrm{P})\big|_{\mathrm{P}\to 0} = \frac{1}{j4} H_o^{(2)}(k_\rho \mathrm{P})\Big|_{\mathrm{P}\to 0} \approx \frac{1}{j4}\left[1 - j\frac{2}{\pi}\left(\mathrm{C} + \ln\frac{k_\rho \mathrm{P}}{2} \right) \right] \tag{3.12}$$

where C is Euler's constant ($\mathrm{C}=0.57721566\ldots$). At the singular point special care must be taken when manipulating the integral representations (equations 3.10 and 3.11). We address this issue in the next two sections.

3.2 Equivalent Integral Representations

In order to simplify the representations given by (3.10) and (3.11), we desire to interchange the order of integration and differentiation in some terms. For this operation to be valid, the Green's function must exist and have continuous first order partial derivatives [11,552]. These conditions exist if the observation point is not <u>on</u> the boundary ℓ. To allow

the interchange, the observation point is assumed to lie in the dielectric region a small distance δ away from ℓ. In Section 3.3 we investigate the case where the observation point approachs the surface $(\delta \rightarrow 0)$.

Consider the first term of (3.10),

$$-\left(\nabla_{tr} \times \oint_{\ell} G^{d}(\rho,\rho')\, M_t(\rho')\, \hat{t}'\, dt'\right) \cdot \hat{z} = -\oint_{\ell} \hat{z} \cdot \left(\nabla_{tr} \times \left(G^{d}(\rho,\rho')\, \hat{t}'\right)\right) M_t(\rho')\, dt'. \tag{3.13}$$

Since ∇_{tr} does not operate on the primed coordinates, the term $\nabla_{tr} \times \left(G^{d} \hat{t}'\right)$ reduces to $\left(\nabla_{tr} G^{d}\right) \times \hat{t}'$. The right hand side of (3.13) now becomes

$$\oint_{\ell} \left(\hat{z} \cdot \left(\nabla_{tr} G^{d}(\rho,\rho')\right) \times \hat{t}'\right) M_t(\rho')\, dt' \ . \tag{3.14}$$

Since $G^{d}(\rho,\rho')$ is a function of $|\rho - \rho'|$ (see 3.7), $\nabla_{tr} G^{d}(\rho,\rho')$ is equivalent to

$$\nabla_{tr}\, G^{d}(\rho,\rho') = -\nabla'_{tr}\, G^{d}(\rho,\rho') \tag{3.15}$$

where ∇'_{tr} operates on the primed (source) coordinates [6,497]. Using our local coordinate system (Fig. 3.3),

$$-\left(\left(\nabla'_{tr}\ G^{d}(\rho,\rho')\right) \times \hat{t}'\right) \cdot \hat{z} = -\left[\left(\frac{\partial G^{d}}{\partial n'} \hat{n}' + \frac{\partial G^{d}}{\partial t'} \hat{t}'\right) \times \hat{t}'\right] \cdot \hat{z} = -\frac{\partial G^{d}}{\partial n'} \ . \tag{3.16}$$

Equation (3.13) now becomes

$$-\left(\nabla_{tr} \times \oint_{\ell} G^{d}(\rho,\rho')\, M_t(\rho')\, \hat{t}'\, dt'\right) \cdot \hat{z} = \oint_{\ell} \frac{\partial G^{d}(\rho,\rho')}{\partial n'}\, M_t(\rho')\, dt'. \tag{3.17}$$

For an expression similar to the third term in (3.10) we have

$$\nabla_{tr}\cdot\oint_{\ell} \mathrm{G}^{\mathrm{d}}(\rho,\rho')\, J_t(\rho')\,\hat{\mathbf{t}}'\,dt' = -\oint_{\ell}\left[\left(\nabla'_{tr}\mathrm{G}^{\mathrm{d}}(\rho,\rho')\right)\cdot\hat{\mathbf{t}}'\right] J_t(\rho')\,dt' \,. \tag{3.18}$$

But,

$$\left[\left(\nabla'_{tr}\,\mathrm{G}^{\mathrm{d}}(\rho,\rho')\right)\cdot\hat{\mathbf{t}}'\right]J_t(\rho') = J_t\,\frac{\partial \mathrm{G}^{\mathrm{d}}}{\partial t'} = \frac{\partial}{\partial t'}\left(J_t\,\mathrm{G}^{\mathrm{d}}\right) - \mathrm{G}^{\mathrm{d}}\frac{\partial J_t}{\partial t'}$$

so (3.18) becomes

$$\nabla_{tr}\cdot\oint_{\ell} \mathrm{G}^{\mathrm{d}}(\rho,\rho')\, J_t(\rho')\hat{\mathbf{t}}'\,dt' = -\oint_{\ell}\frac{\partial}{\partial t'}\left(J_t\,\mathrm{G}^{\mathrm{d}}\right)dt' + \oint_{\ell}\mathrm{G}^{\mathrm{d}}\,\frac{\partial J_t}{\partial t'}\,dt' \,. \tag{3.19}$$

Since the current and the Green's functions are single valued functions, the first term on the right hand side of (3.19) evaluates to zero. Thus, (3.19) becomes

$$\nabla_{tr}\cdot\oint_{\ell} \mathrm{G}^{\mathrm{d}}(\rho,\rho')\, J_t(\rho')\,\hat{\mathbf{t}}'\,dt' = \oint_{\ell}\mathrm{G}^{\mathrm{d}}(\rho,\rho')\,\frac{\partial J_t(\rho')}{\partial t'}\,dt' \,. \tag{3.20}$$

Using (3.17) and (3.20) we may write equation (3.10) as

$$\begin{aligned} E_z^{\mathrm{d}} = {} & \oint_{\ell}\frac{\partial \mathrm{G}^{\mathrm{d}}}{\partial n'}\,M_t\,dt' + \oint_{\ell}\frac{k_{\mathrm{d}}{}^2 - k_z{}^2}{j\omega\epsilon_{\mathrm{d}}^*}\mathrm{G}^{\mathrm{d}}\,J_z\,dt' \\ & - jk_z\oint_{\ell}\frac{1}{j\omega\epsilon_{\mathrm{d}}^*}\mathrm{G}^{\mathrm{d}}\,\frac{\partial J_t}{\partial t'}\,dt' \,. \end{aligned} \tag{3.21}$$

From matching the tangential field components at the interface, we note only the $\hat{\mathbf{z}}$ and $\hat{\mathbf{t}}$ components of the fields are required in our development. By taking the dot product of

(3.11) with $\hat{\mathbf{t}}$ and using the concepts of this section, the following equation is easily derived:

$$E_t^{\mathrm{d}} = -jk_z \oint_{\ell} \mathrm{G}^{\mathrm{d}}\, M_t \left(\hat{\mathbf{n}}' \cdot \hat{\mathbf{t}}\right) dt' + \oint_{\ell} \frac{\partial \mathrm{G}^{\mathrm{d}}}{\partial n} M_z \, dt'$$

$$+ \frac{\partial}{\partial t} \oint_{\ell} \frac{1}{j\omega\epsilon_{\mathrm{d}}^*} \mathrm{G}^{\mathrm{d}} \frac{\partial J_t}{\partial t'} \, dt' - jk_z \frac{\partial}{\partial t} \oint_{\ell} \frac{1}{j\omega\epsilon_{\mathrm{d}}^*} \mathrm{G}^{\mathrm{d}} \, J_z \, dt'$$

$$+ \oint_{\ell} \frac{k_{\mathrm{d}}^{\,2}}{j\omega\epsilon_{\mathrm{d}}^*} \mathrm{G}^{\mathrm{d}} \, J_t \left(\hat{\mathbf{t}}' \cdot \hat{\mathbf{t}}\right) dt' \ . \tag{3.22}$$

3.3 Integral Evaluation at Singular Points

The forms of (3.21) and (3.22) are still not the surface fields needed for the boundary conditions. The observation point must be brought to the surface, where the integrals contain a singularity, making numerical evaluation difficult (if not impossible). To solve this complication, we separate each integral into the sum of two integrals. If we let 2ϵ be a small section of ℓ centered on the singularity, then our integrals may be written as

$$\oint_{\ell} (\,\cdot\,)\, dt' \equiv \int_{\ell - 2\epsilon} (\,\cdot\,)\, dt' + \int_{-\epsilon}^{+\epsilon} (\,\cdot\,)\, dt' \,, \tag{3.23}$$

where $(\,\cdot\,)$ denotes the integrand of interest. The topic of this section is the evaluation of the second integral on the right hand side of (3.23). The remaining integral of (3.23) does not contain a singular point in its interval of integration and may be evaluated using numerical techniques.

To evaluate the singular integral, the following technique is used. As shown in Fig. 3.4, the observation point is located within the dielectric region, centered in the small interval 2ϵ, and displaced a small distance δ away from the boundary ℓ. If δ and ϵ are sufficiently

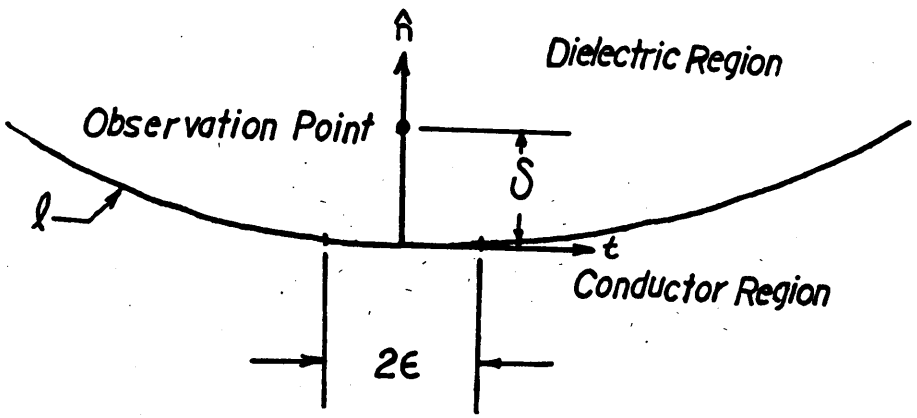

Figure 3.4. Geometry for Singular Point Evaluation.

small, then the singular integrals may be approximated by using small argument expansions of the Green's function and currents. Once the integrals are evaluated, the fields are forced to the surface by imposing the condition $\delta \rightarrow 0$. Finally, the integral contribution is made exact by letting the patch size 2ϵ approach zero, providing a resultant Cauchy principle value form of integration.

The integrals of interest are (see equations 3.7, 3.21, and 3.22)

$$\lim_{\epsilon \rightarrow 0} \lim_{\delta \rightarrow 0} \int_{-\epsilon}^{+\epsilon} I(\rho') \frac{1}{j4} H_o^{(2)}(k_\rho^{\mathrm{d}} |\rho - \rho'|) \, dt' \tag{3.24}$$

$$\lim_{\epsilon \rightarrow 0} \lim_{\delta \rightarrow 0} \int_{-\epsilon}^{+\epsilon} I(\rho') \frac{1}{j4} \frac{\partial}{\partial n} H_o^{(2)}(k_\rho^{\mathrm{d}} |\rho - \rho'|) \, dt' \tag{3.25}$$

$$\lim_{\epsilon \rightarrow 0} \lim_{\delta \rightarrow 0} \int_{-\epsilon}^{+\epsilon} I(\rho') \frac{1}{j4} \frac{\partial}{\partial n'} H_o^{(2)}(k_\rho^{\mathrm{d}} |\rho - \rho'|) \, dt' \tag{3.26}$$

$$\lim_{\epsilon \rightarrow 0} \lim_{\delta \rightarrow 0} \frac{\partial}{\partial t} \int_{-\epsilon}^{+\epsilon} I(\rho') \frac{1}{j4} H_o^{(2)}(k_\rho^{\mathrm{d}} |\rho - \rho'|) \, dt' \tag{3.27}$$

where $I(\rho')$ is either a surface current or a surface derivative of the current. In Appendix B the above integrals are evaluated, allowing equations (3.21) and (3.22) to be written as ,

$$E_z^{\mathrm{d}} = \frac{M_t}{2} + \int_\ell \frac{\partial \mathrm{G}^{\mathrm{d}}}{\partial n'} M_t \, dt' + \int_\ell \frac{k_{\mathrm{d}}{}^2 - k_z{}^2}{j\omega\epsilon_{\mathrm{d}}^*} \mathrm{G}^{\mathrm{d}} \, J_z \, dt'$$

$$- jk_z \int_\ell \frac{1}{j\omega\epsilon_{\mathrm{d}}^*} \mathrm{G}^{\mathrm{d}} \frac{\partial J_t}{\partial t'} \, dt' \tag{3.28}$$

and

$$E_t^d = -\frac{M_z}{2} - jk_z \int_\ell G^d M_t \left(\hat{n}' \cdot \hat{t}\right) dt' + \int_\ell \frac{\partial G^d}{\partial n} M_z \, dt'$$

$$+ \frac{\partial}{\partial t} \int_\ell \frac{1}{j\omega\epsilon_d^*} G^d \frac{\partial J_t}{\partial t'} \, dt' - jk_z \frac{\partial}{\partial t} \int_\ell \frac{1}{j\omega\epsilon_d^*} G^d \, J_z \, dt'$$

$$+ \int_\ell \frac{k_d^2}{j\omega\epsilon_d^*} G^d \, J_t \left(\hat{t}' \cdot \hat{t}\right) dt' \quad . \tag{3.29}$$

The symbol $\int$ signifies that the integral is to exclude the singular point in a Cauchy limiting sense. In the remainder of this thesis (and in the above two equations) the observation point is assumed to be infinitesimally close the boundary ℓ .

To complete our development, we need the representations of the fields in the conductor. If a little care is exercised, these representations may be obtained directly from (3.28) and (3.29). The derivation involves using the equivalence principle for a new problem (Fig. 3.5) which has the actual fields $(\mathbf{E}^c, \mathbf{H}^c)$ in the conductor region and null fields (0,0) in the dielectric region. Also, the dielectric medium is replaced by the conducting medium. To support the postulated field distribution, surface currents must exist on the boundary. These currents are given by

$$\mathbf{J}^c = -\hat{n}' \times \mathbf{H}^c\big|_\ell \tag{3.30}$$

$$\mathbf{M}^c = +\hat{n}' \times \mathbf{E}^c\big|_\ell \, . \tag{3.31}$$

Comparing the above relations with (3.1) and (3.2) we see an apparent minus sign "discrepancy". The minus sign is justified since the direction of the unit normal $\hat{n}'$ is pointed away from the conductor region [1,34]. The currents given by (3.30) and (3.31) radiate into an

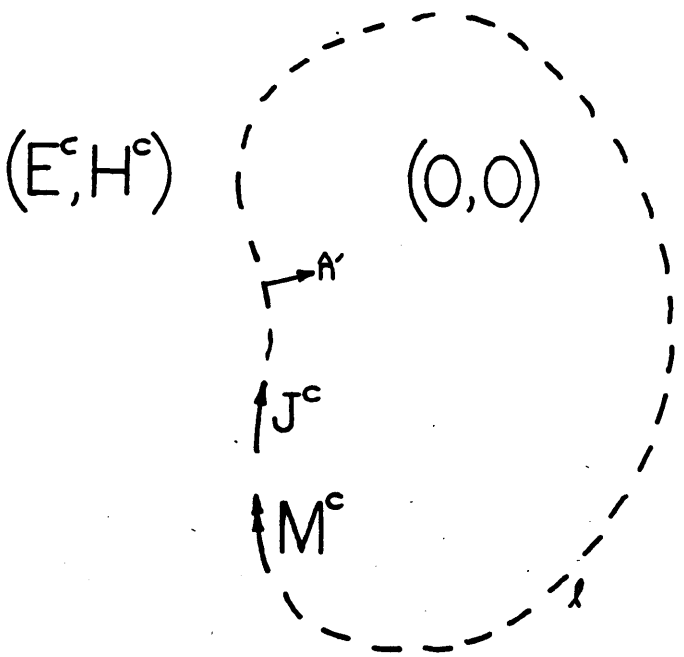

Figure 3.5. Equivalent problem for computing the conductor fields.

isotropic, unbounded, and homogeneous region — the same conditions leading to equations (3.28) and (3.29). To obtain the conductor fields, equations (3.28) and (3.29) must be modified to account for the different currents and media. Specifically, the following substitutions are required:

$$M_t^c \rightarrow M_t \ , \ M_z^c \rightarrow M_z \ , \ J_t^c \rightarrow J_t \ , \ J_z^c \rightarrow J_z \tag{3.32a}$$

$$\epsilon_c^* \rightarrow \epsilon_d^* \ , \ \mu_c^* \rightarrow \mu_d^* \ , \ {k_c}^2 \rightarrow {k_d}^2 \ , \ G^c \rightarrow G^d \tag{3.32b}$$

where,

$${k_c}^2 \equiv \omega^2 \mu_c^* \epsilon_c^* \tag{3.32c}$$

$$G^c(\rho,\rho') \equiv \frac{1}{j4} H_o^{(2)}(k_\rho^c |\rho-\rho'|) \tag{3.32d}$$

$$k_\rho^c \equiv \sqrt{{k_c}^2 - {k_z}^2} \ . \tag{3.32e}$$

We now have,

$$E_z^c = -\frac{M_t^c}{2} + \int_\ell \frac{\partial G^c}{\partial n'} M_t^c \, dt' + \int_\ell \frac{{k_c}^2 - {k_z}^2}{j\omega\epsilon_c^*} G^c \, J_z^c \, dt'$$

$$- jk_z \int_\ell \frac{1}{j\omega\epsilon_c^*} G^c \, \frac{\partial J_t^c}{\partial t'} \, dt' \tag{3.33}$$

and

$$E_t^c = +\frac{M_z^c}{2} - jk_z \int_\ell G^c \, M_t^c \left(\hat{n}' \cdot \hat{t} \right) dt' + \int_\ell \frac{\partial G^c}{\partial n} M_z^c \, dt'$$

$$+ \frac{\partial}{\partial t} \int_\ell \frac{1}{j\omega\epsilon_c^*} G^c \, \frac{\partial J_t^c}{\partial t'} \, dt' - jk_z \frac{\partial}{\partial t} \int_\ell \frac{1}{j\omega\epsilon_c^*} G^c \, J_z^c \, dt'$$

$$+ \int_\ell \frac{{k_c}^2}{j\omega\epsilon_c^*} G^c \, J_t^c \left(\hat{t}' \cdot \hat{t} \right) dt' \ . \tag{3.34}$$

We note that the terms (see 3.28 and 3.29)

$$\frac{M_t}{2} \text{ and } \frac{M_z}{2} \tag{3.35}$$

and the corresponding terms in (3.33) and (3.34) appear to have conflicting signs. Recall, the above terms resulted from the integrals (3.25) and (3.26). In the calculation of (3.25) and (3.26), the derivatives were calculated with the observation point approaching ℓ from within the dielectric region. However, the conductor fields must be forced to approach the boundary from within the conductor region. In this case the normal derivatives are taken on the opposite side of ℓ, creating the negative signs in question. The proof is straightforward with the observation point located at $n = -\delta$ (see Fig. 3.4) and following the approach given in Appendix B.

3.4 Integral Equation Solution to the Waveguide Problem

Unless the conductors are perfect, the $\hat{\mathbf{t}}$ and $\hat{\mathbf{z}}$ components of the fields are continuous across the boundary [1,34]. This condition requires

$$E_z^{\mathsf{d}} = E_z^{\mathsf{c}} \text{ and } E_t^{\mathsf{d}} = E_t^{\mathsf{c}} \tag{3.36a}$$

and

$$H_z^{\mathsf{d}} = H_z^{\mathsf{c}} \text{ and } H_t^{\mathsf{d}} = H_t^{\mathsf{c}} \,. \tag{3.36b}$$

Using (3.36) with (3.28), (3.29), (3.33), and (3.34) gives,

$$\begin{aligned} &\frac{M_t}{2} + \int_\ell \frac{\partial \mathrm{G}^{\mathsf{d}}}{\partial n'} M_t \, dt' + \int_\ell \frac{{k_{\mathsf{d}}}^2 - {k_z}^2}{j\omega\epsilon_{\mathsf{d}}^*} \mathrm{G}^{\mathsf{d}} \, J_z \, dt' \\ &- jk_z \int_\ell \frac{1}{j\omega\epsilon_{\mathsf{d}}^*} \mathrm{G}^{\mathsf{d}} \frac{\partial J_t}{\partial t'} \, dt' = -\frac{M_t^{\mathsf{c}}}{2} + \int_\ell \frac{\partial \mathrm{G}^{\mathsf{c}}}{\partial n'} M_t^{\mathsf{c}} \, dt' \\ &+ \int_\ell \frac{{k_{\mathsf{c}}}^2 - {k_z}^2}{j\omega\epsilon_{\mathsf{c}}^*} \mathrm{G}^{\mathsf{c}} \, J_z^{\mathsf{c}} \, dt' - jk_z \int_\ell \frac{1}{j\omega\epsilon_{\mathsf{c}}^*} \mathrm{G}^{\mathsf{c}} \frac{\partial J_t^{\mathsf{c}}}{\partial t'} \, dt' \end{aligned} \tag{3.37}$$

and

$$-\frac{M_z}{2} - jk_z \int_\ell G^d M_t \left(\hat{n}' \cdot \hat{t}\right) dt' + \int_\ell \frac{\partial G^d}{\partial n} M_z \, dt'$$

$$+ \frac{\partial}{\partial t} \int_\ell \frac{1}{j\omega\epsilon_d^*} G^d \frac{\partial J_t}{\partial t'} \, dt' - jk_z \frac{\partial}{\partial t} \int_\ell \frac{1}{j\omega\epsilon_d^*} G^d J_z \, dt'$$

$$+ \int_\ell \frac{k_d^2}{j\omega\epsilon_d^*} G^d J_t \left(\hat{t}' \cdot \hat{t}\right) dt' = + \frac{M_z^c}{2} - jk_z \int_\ell G^c M_t^c \left(\hat{n}' \cdot \hat{t}\right) dt'$$

$$+ \int_\ell \frac{\partial G^c}{\partial n} M_z^c \, dt' + \frac{\partial}{\partial t} \int_\ell \frac{1}{j\omega\epsilon_c^*} G^c \frac{\partial J_t^c}{\partial t'} \, dt'$$

$$- jk_z \frac{\partial}{\partial t} \int_\ell \frac{1}{j\omega\epsilon_c^*} G^c J_z^c \, dt' + \int_\ell \frac{k_c^2}{j\omega\epsilon_c^*} G^c J_t^c \left(\hat{t}' \cdot \hat{t}\right) dt' \, . \tag{3.38}$$

From the continuity requirement (3.36) and the equivalent source relations (3.1), (3.2), (3.30) and (3.31), we find that $\mathbf{J}^d \equiv \mathbf{J} = -\mathbf{J}^c$ and $\mathbf{M}^d \equiv \mathbf{M} = -\mathbf{M}^c$; which is equivalent to,

$$J_z = -J_z^c \, , \quad J_t = -J_t^c \tag{3.39}$$

and

$$M_z = -M_z^c \, , \quad M_t = -M_t^c \, . \tag{3.40}$$

Using (3.39) and (3.40) and collecting like terms, (3.37) and (3.38) may be expressed as,

$$\int_\ell \left(\frac{\partial G^d}{\partial n'} + \frac{\partial G^c}{\partial n'} \right) M_t \, dt'$$

$$+ \int_\ell \left(\frac{k_d^2 - k_z^2}{j\omega\epsilon_d^*} G^d + \frac{k_c^2 - k_z^2}{j\omega\epsilon_c^*} G^c \right) J_z \, dt'$$

$$- jk_z \int_\ell \left(\frac{1}{j\omega\epsilon_d^*} G^d + \frac{1}{j\omega\epsilon_c^*} G^c \right) \frac{\partial J_t}{\partial t'} \, dt' = 0 \tag{3.41}$$

and

$$-jk_z \int_\ell \left(G^d + G^c\right) M_t \left(\hat{n}' \cdot \hat{t}\right) dt' + \int_\ell \left(\frac{\partial G^d}{\partial n} + \frac{\partial G^c}{\partial n}\right) M_z \, dt'$$

$$+ \frac{\partial}{\partial t} \int_\ell \left(\frac{1}{j\omega\epsilon_d^*} G^d + \frac{1}{j\omega\epsilon_c^*} G^c\right) \frac{\partial J_t}{\partial t'} \, dt'$$

$$- jk_z \frac{\partial}{\partial t} \int_\ell \left(\frac{1}{j\omega\epsilon_d^*} G^d + \frac{1}{j\omega\epsilon_c^*} G^c\right) J_z \, dt'$$

$$+ \int_\ell \left(\frac{k_d^2}{j\omega\epsilon_d^*} G^d + \frac{k_c^2}{j\omega\epsilon_c^*} G^c\right) J_t \left(\hat{t}' \cdot \hat{t}\right) dt' = 0 \ . \tag{3.42}$$

Equations (3.41) and (3.42) contain four unknown functions — J_z , J_t , M_z , and M_t . To completely specify the problem, two more independent equations are required. These equations are obtained by matching the $\hat{t}$ and $\hat{z}$ components of the magnetic field at the boundary. From the duality principle [1,98], the magnetic field equations are obtained by using the following substitutions in (3.41) and (3.42): $J_z \rightarrow M_z$, $J_t \rightarrow M_t$, $M_z \rightarrow -J_z$, $M_t \rightarrow -J_t$, $\epsilon_d^* \rightarrow \mu_d^*$, $\epsilon_c^* \rightarrow \mu_c^*$, $\mu_d^* \rightarrow \epsilon_d^*$, and $\mu_c^* \rightarrow \epsilon_c^*$. The resulting equations are

$$-\int_\ell \left(\frac{\partial G^d}{\partial n'} + \frac{\partial G^c}{\partial n'}\right) J_t \, dt'$$

$$+ \int_\ell \left(\frac{k_d^2 - k_z^2}{j\omega\mu_d^*} G^d + \frac{k_c^2 - k_z^2}{j\omega\mu_c^*} G^c\right) M_z \, dt'$$

$$- jk_z \int_\ell \left(\frac{1}{j\omega\mu_d^*} G^d + \frac{1}{j\omega\mu_c^*} G^c\right) \frac{\partial M_t}{\partial t'} \, dt' = 0 \tag{3.43}$$

and

$$+jk_z \int_\ell \left(G^d + G^c\right) J_t \left(\hat{n}' \cdot \hat{t}\right) dt' - \int_\ell \left(\frac{\partial G^d}{\partial n} + \frac{\partial G^c}{\partial n}\right) J_z \, dt'$$

$$+ \frac{\partial}{\partial t} \int_\ell \left(\frac{1}{j\omega\mu_d^*} G^d + \frac{1}{j\omega\mu_c^*} G^c\right) \frac{\partial M_t}{\partial t'} \, dt'$$

$$- jk_z \frac{\partial}{\partial t} \int_\ell \left(\frac{1}{j\omega\mu_d^*} G^d + \frac{1}{j\omega\mu_c^*} G^c\right) M_z \, dt'$$

$$+ \int_\ell \left(\frac{k_d^2}{j\omega\mu_d^*} G^d + \frac{k_c^2}{j\omega\mu_c^*} G^c\right) M_t \left(\hat{t}' \cdot \hat{t}\right) dt' = 0 \ . \tag{3.44}$$

Our ultimate goal is to develop a numerical solution to the set of coupled integral equations (3.41 through 3.44). Given the material parameters (ϵ_d^*, μ_d^*, ϵ_c^*, and μ_c^*), the problem is to find the values of k_z which satisfy (3.41) through (3.44). The reverse problem is also of interest — if k_z is known (i.e. measured) then allowable values for the material parameters are to be determined. In Chapter 4 the integral equations are cast into a numerical form.

3.5 Extension of the Waveguide Development to the Transmission Line Problem

The analytical development for the transmission line problem (Fig. 3.6) follows directly from the waveguide results of Section 3.4. In the waveguide problem we had four unknown currents (J_t, J_z, M_t, and, M_z) flowing on a single conducting surface. However, in the transmission line problem we have two conducting surfaces and we expect eight currents (four at each conducting surface). We designate these currents as (J_t^o, J_z^o, M_t^o, M_z^o) and (J_t^i, J_z^i, M_t^i, and M_z^i) where the superscripts o and i refer to the currents on the outer and inner conductors, respectively.

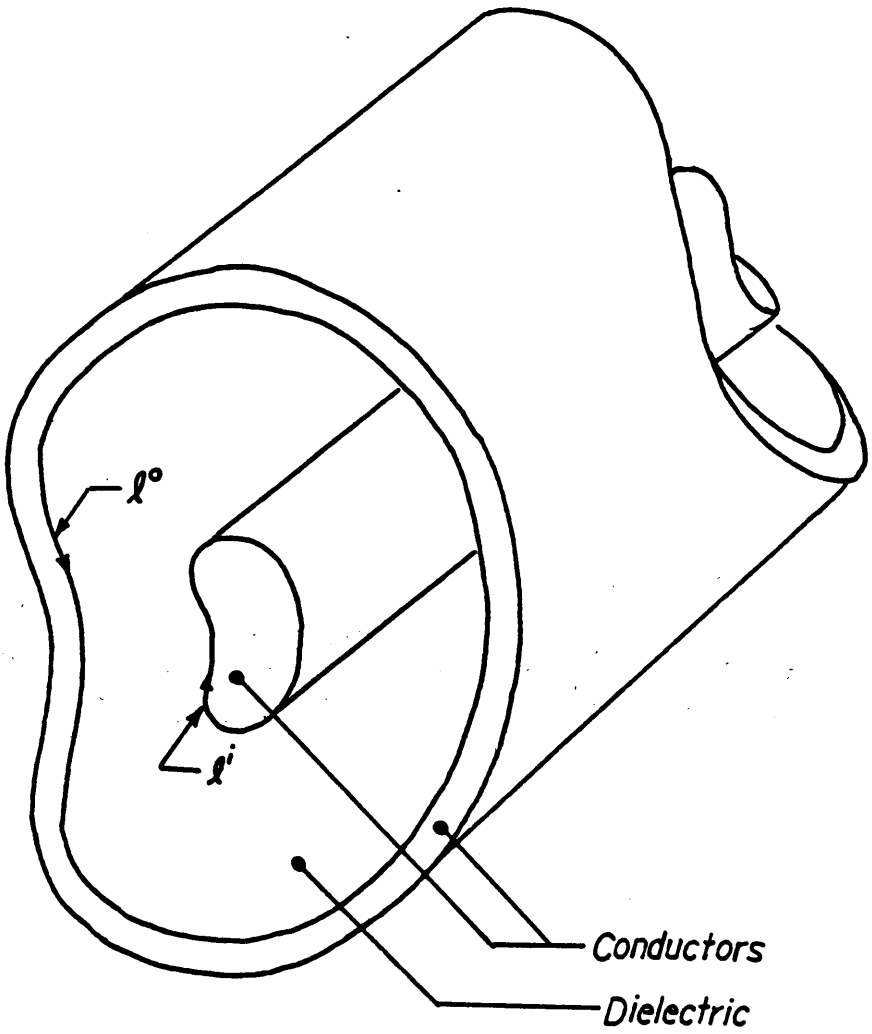

Figure 3.6. Transmission line.

To obtain a solution to the transmission line problem we must obtain eight independent equations. As in the waveguide problem, these equations are derived by matching the $\hat{t}$ and $\hat{z}$ field components at the conducting surfaces. Specifically, the procedure involves matching E_t, H_t, E_z, and H_z at the two boundaries ℓ^o and ℓ^i (Fig. 3.6).

Using the equivalence principle, we find that the field equations within each conducting region are the same as those given by equations (3.33) and (3.34). In the dielectric region the equivalence principal must be applied at each conducting surface. For example, the actual fields are postulated within the dielectric while null fields are postulated within the inner and outer conductors. To satisfy the boundary conditions (see section 3.1) surface currents must exist on both boundaries. The vector potential representations of the fields (e.g. equation 3.3) are still valid in the dielectric region; however, to account for the currents on both boundaries, the Helmholtz integral solutions (3.5 and 3.6) are modified as follows:

$$\mathbf{A} = \oint_{\ell^o} \mathbf{J}^o(\rho')\, G^d(\rho,\rho')\, dt' + \oint_{\ell^i} \mathbf{J}^i(\rho')\, G^d(\rho,\rho')\, dt' \tag{3.45}$$

$$\mathbf{F} = \oint_{\ell^o} \mathbf{M}^o(\rho')\, G^d(\rho,\rho')\, dt' + \oint_{\ell^i} \mathbf{M}^i(\rho')\, G^d(\rho,\rho')\, dt' \,. \tag{3.46}$$

If we match the $\hat{z}$ components of the electric field at some point on the outer conductor and proceed as in sections 3.1 through 3.4, we obtain the following integral equation:

$$\oint_{\ell^o} \left(\frac{\partial G^d}{\partial n'} + \frac{\partial G^c}{\partial n'} \right)^{o,o} M_t^o\, (dt')^o$$

$$+ \oint_{\ell^o} \left(\frac{k_d^2 - k_z^2}{j\omega\epsilon_d^*} G^d + \frac{k_c^2 - k_z^2}{j\omega\epsilon_c^*} G^c \right)^{o,o} J_z^o\, (dt')^o$$

$$- jk_z \oint_{\ell^o} \left(\frac{1}{j\omega\epsilon_d^*} G^d + \frac{1}{j\omega\epsilon_c^*} G^c \right)^{o,o} \frac{\partial J_t^o}{\partial t'}\, (dt')^o$$

$$+\oint_{\ell^i}\left(\frac{\partial G^d}{\partial n'}\right)^{o,i} M_t^i\,(dt')^i+\oint_{\ell^i}\left(\frac{k_d^{\,2}-k_z^{\,2}}{j\omega\epsilon_d^*}\,G^d\right)^{o,i} J_z^i\,(dt')^i$$

$$-jk_z\oint_{\ell^i}\left(\frac{1}{j\omega\epsilon_d^*}G^d\right)^{o,i}\frac{\partial J_t^i}{\partial t'}\,(dt')^i=0 \qquad (3.47)$$

where the single superscript, o or i, represents the appropriate quantity at the outer or inner surface, respectively. The double superscripts designate the surface at which the observation point is located and the surface over which the source exists. For example, the double superscript (o,i) implies the observation point is located at some point on the outer surface ℓ^o and the source exists on the inner surface ℓ^i. If we match the $\hat{t}$ components of the electric field at some point on the outer surface, we obtain

$$-jk_z\oint_{\ell^o}\left(G^d+G^c\right)^{o,o} M_t^o\,(\hat{n}'\cdot\hat{t})^{o,o}\,(dt')^o$$

$$+\oint_{\ell^o}\left(\frac{\partial G^d}{\partial n}+\frac{\partial G^c}{\partial n}\right)^{o,o} M_z^o\,(dt')^o$$

$$+\frac{\partial}{\partial t}\oint_{\ell^o}\left(\frac{1}{j\omega\epsilon_d^*}G^d+\frac{1}{j\omega\epsilon_c^*}G^c\right)^{o,o}\frac{\partial J_t^o}{\partial t'}\,(dt')^o$$

$$-jk_z\frac{\partial}{\partial t}\oint_{\ell^o}\left(\frac{1}{j\omega\epsilon_d^*}G^d+\frac{1}{j\omega\epsilon_c^*}G^c\right)^{o,o} J_z^o\,(dt')^o$$

$$+\oint_{\ell^o}\left(\frac{k_d^{\,2}}{j\omega\epsilon_d^*}G^d+\frac{k_c^{\,2}}{j\omega\epsilon_c^*}G^c\right)^{o,o} J_t^o\,(\hat{t}'\cdot\hat{t})^{o,o}\,(dt')^o$$

$$-jk_z\oint_{\ell^i}\left(G^d\right)^{o,i} M_t^i\,(\hat{n}'\cdot\hat{t})^{o,i}\,(dt')^i+\oint_{\ell^i}\left(\frac{\partial G^d}{\partial n}\right)^{o,i} M_z^i\,(dt')^i$$

$$+\frac{\partial}{\partial t}\oint_{\ell^i}\left(\frac{1}{j\omega\epsilon_d^*}G^d\right)^{o,i}\frac{\partial J_t^i}{\partial t'}\,(dt')^i$$

$$-jk_z \frac{\partial}{\partial t} \oint_{\ell^i} \left(\frac{1}{j\omega\epsilon_d^*} G^d \right)^{o,i} J_z^i (dt')^i$$

$$+ \oint_{\ell^i} \left(\frac{k_d^2}{j\omega\epsilon_d^*} G^d \right)^{o,i} J_t^i (\hat{t}' \cdot \hat{t})^{o,i} (dt')^i = 0 \quad . \tag{3.48}$$

By simply switching the superscripts (o→i and i→o) in equations (3.47) and (3.48) we can obtain two more independent equations. The resulting equations are equivalent to those derived by matching the $\hat{t}$ and $\hat{z}$ components of the electric field at the inner conductor. The final four equations are found by matching the $\hat{t}$ and $\hat{z}$ components of the magnetic field at the two surfaces. Once again, these equations may be easily obtained by applying the duality principle to the electric field equations.

Chapter 4

Numerical Implementation

4.1 Introduction

In this chapter we numerically solve the waveguide problem developed in the previous chapter. Specifically, the four coupled integral equations derived in the last chapter are to be solved with the well-known Method of Moments (MOM) technique [12]. We shall see that the MOM technique reduces the coupled integral equations into a set of simultaneous linear equations, which may be solved by a number of well-known techniques (e.g. LU decomposition).

4.2 Introduction to the Method of Moments

Consider an integral equation of the form

$$\int_{\ell} \mathrm{K}(u,u')\, f(u')\, du' = g(u) \tag{4.1}$$

where the functions $\mathrm{K}(u,u')$ and $g(u)$ are given and $f(u')$ is some unknown function. An integral equation of this form is called a Fredholm equation of the first kind. One approach to solve such an equation is to expand $f(u')$ in a complete set (generally, an infinite number) of known basis functions [16,50]. If we define $\Phi_n(u')$ as the n^{th} basis function, then the function $f(u')$ may be expressed as

$$f(u') = \sum_{n=1}^{\infty} A_n \Phi_n(u') \,, \tag{4.2}$$

where A_n is an unknown constant (complex amplitude). If n is restricted to a finite number N, (4.2) is equivalent to finding the projection of $f(u')$ onto a finite N dimensional space represented by the N functions $\Phi_n(u')$ [16,50]. If we define the resulting error term as $\varepsilon(u')$ then (4.2) may be expressed as,

$$f(u') = \sum_{n=1}^{N} A_n \Phi_n(u') + \varepsilon(u') \,. \tag{4.3}$$

Upon substituting (4.3) into (4.1) we obtain

$$\int_{\ell'} K(u,u') \sum_{n=1}^{N} A_n \Phi_n(u') \, du' + \int_{\ell'} K(u,u') \, \varepsilon(u') \, du' = g(u) \tag{4.4}$$

or,

$$\sum_{n=1}^{N} A_n \int_{\ell'} K(u,u') \, \Phi_n(u') \, du' + \int_{\ell'} K(u,u') \, \varepsilon(u') \, du' = g(u) \,. \tag{4.5}$$

Equation (4.5) has N unknown amplitudes A_n. To generate a total of N independent equations having N unknowns, we choose N independent functions $W_m(u)$, m = [1...N]. These functions, commonly called testing or weighting functions, are then multiplied by both sides of (4.5) and integrated with respect to u to give,

$$\sum_{n=1}^{N} A_n \int_{\ell} W_m(u) \left(\int_{\ell'} K(u,u') \, \Phi_n(u') \, du' \right) du = \int_{\ell} W_m(u) \, g(u) \, du \,, \; m = [1...N] \tag{4.6}$$

or,

$$\sum_{n=1}^{N} A_n \int_{\ell'} \Phi_n(u') \left(\int_{\ell} W_m(u) \, K(u,u') \, du \right) du' = \int_{\ell} W_m(u) \, g(u) \, du \,, \; m = [1...N] \tag{4.7}$$

where the projection of the error term onto the chosen N dimensional space has been forced to zero. To reduce the significance of the error term, the basis function $\Phi_n(u')$ should be a reasonable approximation of the unknown distribution.

Equation (4.7) may be compactly written as

$$\sum_{n=1}^{N} Z_{mn}\, A_n = V_m, \quad m=[1...N]\,, \tag{4.8}$$

where

$$Z_{mn} \equiv \int_{\ell'} \Phi_n(u') \left(\int_{\ell} \mathcal{W}_m(u)\, K(u,u')\, du \right) du'\,, \tag{4.9}$$

and

$$V_m \equiv \int_{\ell} \mathcal{W}_m(u)\, g(u)\, du\,. \tag{4.10}$$

In matrix notation we have

$$[Z]\cdot[A] = [V] \tag{4.11}$$

where $[Z]$, $[A]$, and $[V]$ are $N \times N$, $N \times 1$, and $N \times 1$ matrices respectively. Once the elements of $[Z]$ and $[V]$ are obtained, the unknown coefficients $[A]$ may be determined by using an algorithm such as LU decomposition.

The choice of expansion and testing (weighting) functions is an important topic. In the above discussion it was noted that the expansion function should reasonably approximate the unknown function. The testing function should be chosen such that small variations in the testing location (the testing function's interval of integration) does not cause significant changes in $[A]$. The particular choices should also represent a balance between accuracy and efficiency [10,187]. In general, clear-cut rules on this topic do not exist. Some widely used expansion functions include the pulse and triangular functions (see the next section and [10,188]), while comonly used testing functions include the pulse and Dirac delta functions.

4.3 Moment Method Solution of the Waveguide Problem

The first step in numerically solving the problem of interest is to approximate the boundary ℓ by a discrete set of N points: t'_n, $n = [1,\ldots,N]$ (Fig. 4.1). By connecting adjacent points with a straight line we form N linear segments. The segments are referenced as $\Delta\ell_n$, $n = [1,\ldots,N]$ where the n^{th} segment is defined by the points t'_n and t'_{n+1}. These segments, having the lengths Δ_n, $n = [1,\ldots,N]$, are characterized by a set of local coordinate systems having constant tangential and normal vectors.

Next, we approximate the currents by defining basis functions along each segment. From equations (3.41) through (3.44) we find that the current functions we must approximate have the forms

$$I_z(t'), \qquad I_t(t'), \qquad \text{and} \qquad \frac{\partial I_t(t')}{\partial t'}, \tag{4.12}$$

where $I_z(t')$ and $I_t(t')$ represent either an electric or magnetic current. For simplicity we shall expand the currents represented by $I_z(t')$ by a summation of pulse functions. Specifically, we have

$$I_z(t') = \sum_{n=1}^{N} I_n^z P_n(t'), \quad P_n(t') = \begin{cases} 1 & \text{for } t' \text{ in } \Delta\ell_n \\ 0 & \text{elsewhere} \end{cases} \tag{4.13}$$

where the I_n^z's are complex amplitude coefficients. The pulse expansion of (4.13) is equivalent to a "stair-step" approximation of $I_z(t')$ as shown in Fig. 4.2. Since we must approximate $I_t(t')$ and its derivative, the pulse function expansion is not appropriate for this current. We need an expansion function that gives a continuous approximation to the current. A relatively

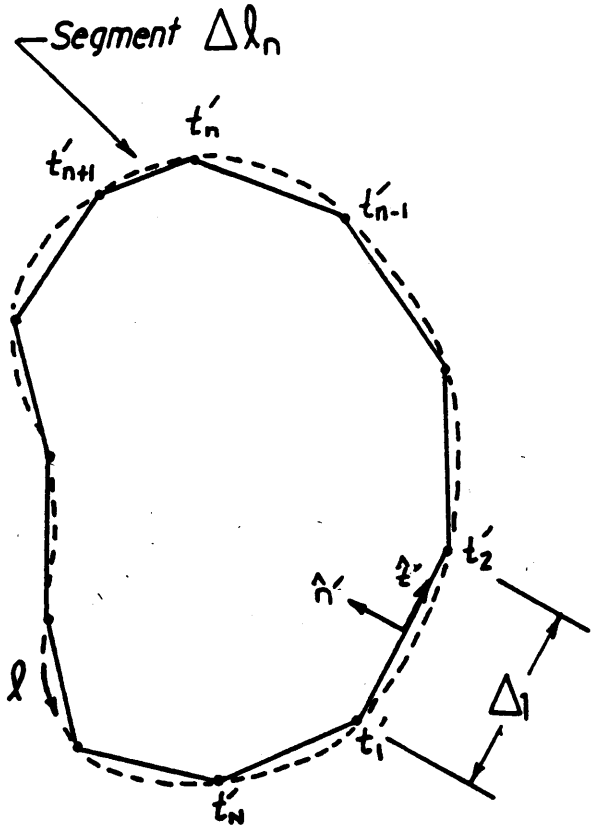

Figure 4.1. Discretization of boundary.

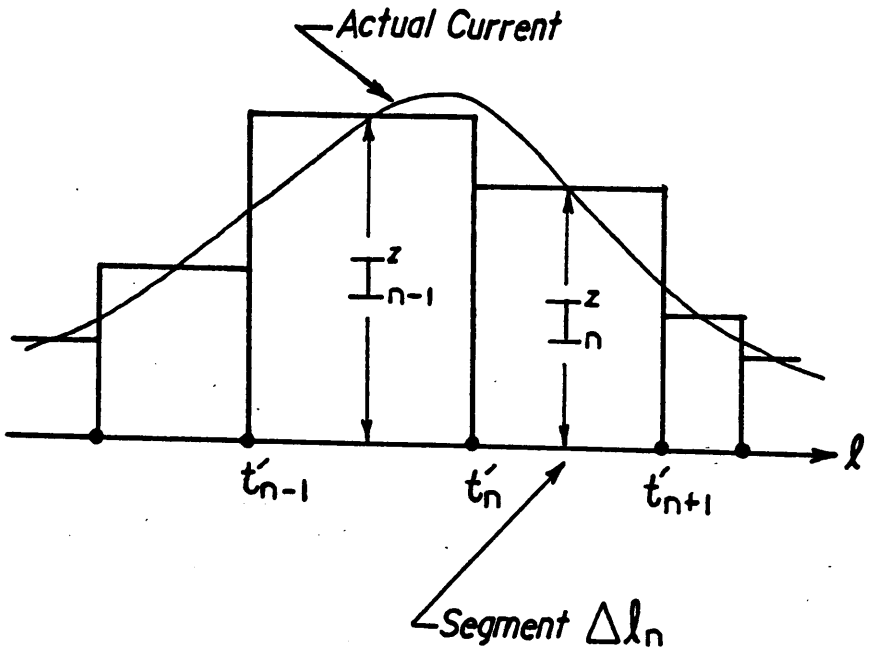

Figure 4.2. Pulse function expansion.

simple expansion meeting these specifications is the series of overlapping triangle functions (Fig. 4.3)

$$I_t(t') = \sum_{n=1}^{N} I_n^t \left(1 - \frac{|t' - t_n'|}{\Delta}\right) P_{2n}(t') \tag{4.14}$$

where,

$$P_{2n}(t') = \begin{cases} 1 & \text{for } t' \text{ in } \Delta\ell_{n-1} \text{ or } \Delta\ell_n \\ 0 & \text{elsewhere} \end{cases}$$

and,

$$\Delta = \begin{cases} \Delta_{n-1} \text{ (length of segment } \Delta\ell_{n-1}) & \text{for } t' \text{ in } \Delta\ell_{n-1} \\ \Delta_n \text{ (length of segment } \Delta\ell_n) & \text{for } t' \text{ in } \Delta\ell_n \end{cases}$$

The expansion of (4.14) is equivalent to a approximating $I_t(t')$ by a linear interpolation between grid points (Fig. 4.4).

Upon substituting the current expansions (4.13) and (4.14) into the the integral equation (3.41), we obtain

$$\int_\ell \left(\frac{\partial G^d}{\partial n'} + \frac{\partial G^c}{\partial n'}\right) \sum_{n=1}^{N} M_n^t \left(1 - \frac{|t' - t_n'|}{\Delta}\right) P_{2n}(t')\, dt'$$

$$+ \int_\ell \left(\frac{k_d^2 - k_z^2}{j\omega\epsilon_d^*} G^d + \frac{k_c^2 - k_z^2}{j\omega\epsilon_c^*} G^c\right) \sum_{n=1}^{N} J_n^z P_n(t')\, dt'$$

$$-jk_z \int_\ell \left(\frac{1}{j\omega\epsilon_d^*} G^d + \frac{1}{j\omega\epsilon_c^*} G^c\right) \frac{\partial}{\partial t'} \sum_{n=1}^{N} J_n^t \left(1 - \frac{|t' - t_n'|}{\Delta}\right) P_{2n}(t')\, dt' = 0 \tag{4.15}$$

where M_n^t, J_n^z, and J_n^t are the n^{th} expansion coefficients for the currents $M_t(t')$, $J_z(t')$, and

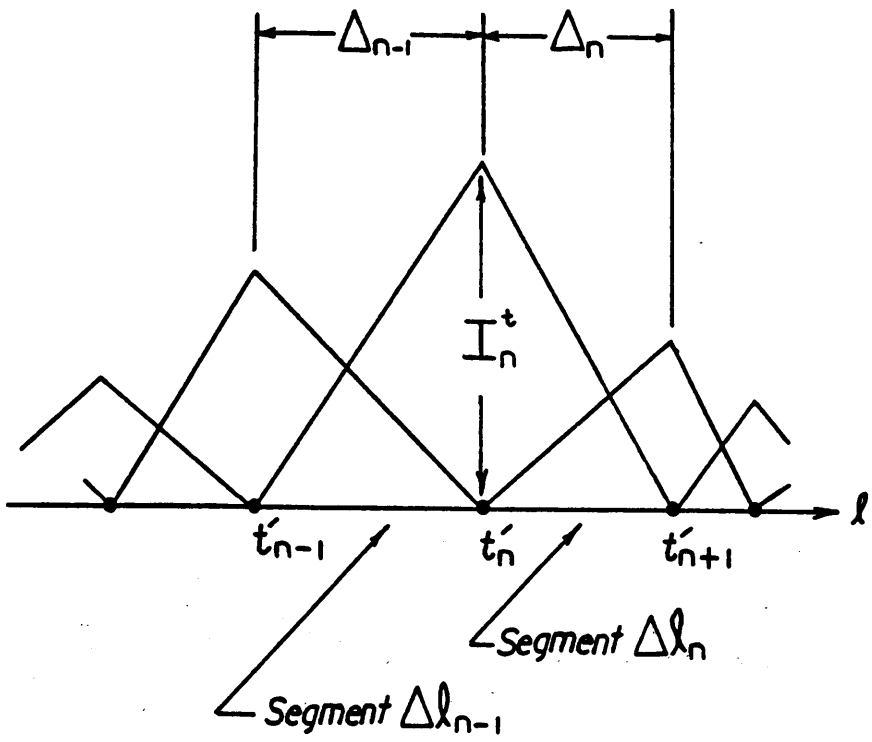

Figure 4.3. Overlapping triangle function expansion.

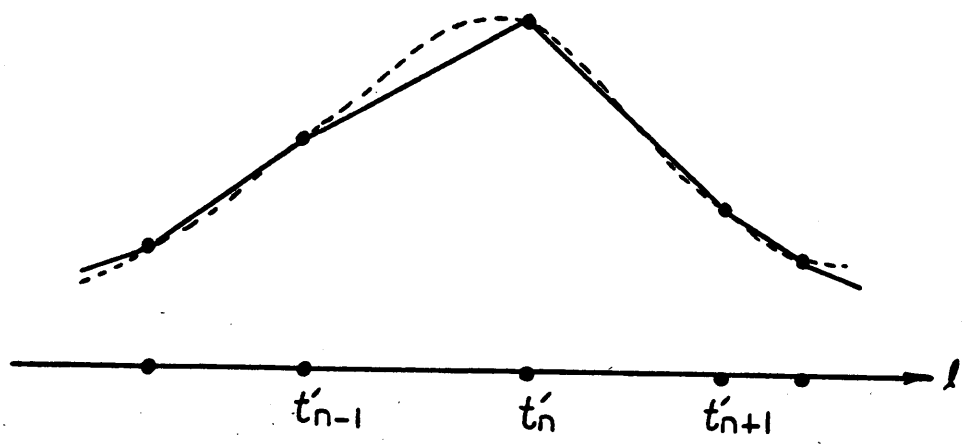

Figure 4.4. Linear approximation of current using the overlapping triangle function expansion.

$J_t(t')$, respectively. In the discussion that follows, the observation point will be designated as t (recall that this point is on the surface ℓ). As explained in section 4.2, we use N independent weighting (testing) functions to generate N independent equations. For simplicity, we let the weighting function for (4.15) be given by

$$\mathcal{W}_m(t) = \delta\left(t - t'_m - \frac{\Delta_m}{2}\right) \ , \ m = [1...N] \ . \tag{4.16}$$

In words, (4.16) states that the weighting function for (4.15) is a delta function that is located at the midpoint of the segment defined by the grid points t'_m and t'_{m+1}. Next, the product of (4.16) and (4.15) is integrated with respect to t. If the segment of integration is the chosen to be $\Delta\ell_m$, we obtain

$$\int_{t_m'}^{t'_{m+1}} (\text{equation 4.15})\ \delta\left(t - t'_m - \frac{\Delta_m}{2}\right) dt, \ m = [1...N] \ . \tag{4.17}$$

In Appendix C we show that (4.17) is equivalent to

$$\sum_{n=1}^{N} M_n^t \left(A_{mn}^d + A_{mn}^c\right)$$

$$+ \sum_{n=1}^{N} J_n^z \left(\frac{k_d^2 - k_z^2}{j\omega\epsilon_d^*} B_{mn}^d + \frac{k_c^2 - k_z^2}{j\omega\epsilon_c^*} B_{mn}^c\right)$$

$$- jk_z \sum_{n=1}^{N} J_n^t \left(\frac{1}{j\omega\epsilon_d^*} C_{mn}^d + \frac{1}{j\omega\epsilon_c^*} C_{mn}^c\right) = 0 \ , \quad m = [1...N] \tag{4.18}$$

where the "constants" $A_{mn}^{d(c)}$, $B_{mn}^{d(c)}$, $C_{mn}^{d(c)}$, are defined in the appendix. By inspection, the

numerical form of the dual equation (3.43) is

$$-\sum_{n=1}^{N} J_n^t \left(A_{mn}^d + A_{mn}^c \right)$$

$$+\sum_{n=1}^{N} M_n^z \left(\frac{k_d^2 - k_z^2}{j\omega\mu_d^*} B_{mn}^d + \frac{k_c^2 - k_z^2}{j\omega\mu_c^*} B_{mn}^c \right)$$

$$-jk_z \sum_{n=1}^{N} M_n^t \left(\frac{1}{j\omega\mu_d^*} C_{mn}^d + \frac{1}{j\omega\mu_c^*} C_{mn}^c \right) = 0 \,, \quad m = [1 \ldots N] \,. \tag{4.19}$$

To enhance the accuracy of the results, pulse functions are used as the weighting functions for the transverse field equations (3.42) and (3.44) [5,318]. These pulse functions, which are centered at the grid point locations, may be stated mathematically as (see Fig. 4.5)

$$\mathcal{W}_m(t) = P_m(t) = \begin{cases} 1 \text{ for } t_{m-} \leq t \leq t_{m+} \\ 0 \text{ elsewhere} \end{cases} \,, \quad m = [1 \ldots N] \tag{4.20}$$

where t_{m-} is the midpoint of segment $\Delta\ell_{m-1}$ and t_{m+} is the midpoint of segment $\Delta\ell_m$. Using the current expansions (4.13 and 4.14) and the weighting function (4.20), the numerical form of (3.42) may be written as (see Appendix C),

$$-jk_z \sum_{n=1}^{N} M_n^t \left(D_{mn}^d + D_{mn}^c \right) + \sum_{n=1}^{N} M_n^z \left(E_{mn}^d + E_{mn}^c \right)$$

$$+\sum_{n=1}^{N} J_n^t \left(\frac{1}{j\omega\epsilon_d^*} F_{mn}^d + \frac{1}{j\omega\epsilon_c^*} F_{mn}^c \right)$$

$$-jk_z \sum_{n=1}^{N} J_n^z \left(\frac{1}{j\omega\epsilon_d^*} G_{mn}^d + \frac{1}{j\omega\epsilon_c^*} G_{mn}^c \right)$$

$$+\sum_{n=1}^{N} J_n^t \left(\frac{k_d^2}{j\omega\epsilon_d^*} H_{mn}^d + \frac{k_c^2}{j\omega\epsilon_c^*} H_{mn}^c \right) = 0 \,, \quad m = [1 \ldots N] \,. \tag{4.21}$$

By inspection, the numerical equivalent of (4.21) for the dual equaton (3.44) is given by

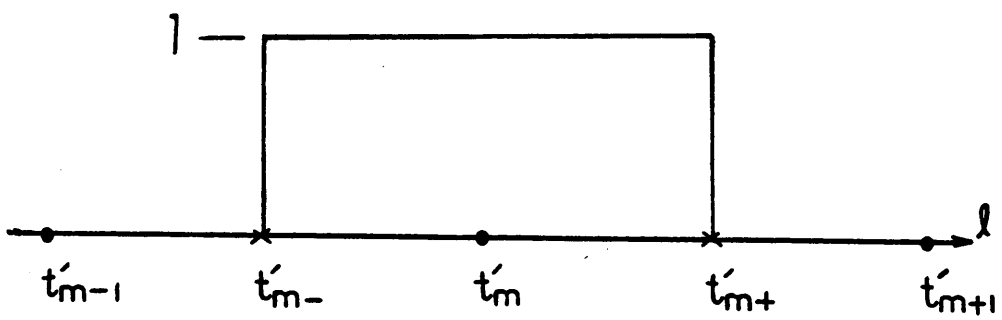

Figure 4.5. Weighting function for the transverse field equations.

the equation

$$+jk_z \sum_{n=1}^{N} J_n^t \left(D_{mn}^d + D_{mn}^c \right) - \sum_{n=1}^{N} J_n^z \left(E_{mn}^d + E_{mn}^c \right)$$

$$+ \sum_{n=1}^{N} M_n^t \left(\frac{1}{j\omega\mu_d^*} F_{mn}^d + \frac{1}{j\omega\mu_c^*} F_{mn}^c \right)$$

$$- jk_z \sum_{n=1}^{N} M_n^z \left(\frac{1}{j\omega\mu_d^*} G_{mn}^d + \frac{1}{j\omega\mu_c^*} G_{mn}^c \right)$$

$$+ \sum_{n=1}^{N} M_n^t \left(\frac{k_d^{\,2}}{j\omega\mu_d^*} H_{mn}^d + \frac{k_c^{\,2}}{j\omega\mu_c^*} H_{mn}^c \right) = 0 \quad , \quad m = [1 \ldots N] \quad . \tag{4.22}$$

From Appendix C we note that the various "constant" terms (A_{mn}^d, A_{mn}^c, B_{mn}^d, B_{mn}^c, C_{mn}^d, etc...) involve integrating a zeroth (or first) order Hankel function of the second kind. These integrals are not tabulated and must be computed via numerical integration. The technique of choice is Simpson's approach [13,110]. This numerical integration "workhorse" is easy to implement and reasonably efficient [13,110]. Naturally, to obtain an accurate approximation of the integral, a substantial number of integrand (Hankel functions) evaluations are required. These evaluations are obtained by one of two techniques. If the magnitude of the argument is less than 10.0, we use the power series form of the appropriate Hankel function [2,959]; if the argument magnitude is greater than 10.0, we use the asymptotic approximation [2,962].

Using matrix notation, equations (4.18), (4.19), (4.21), and (4.22) may be compactly written as

$$\begin{bmatrix} [\![Z_{11}]\!] & \cdots & [\![Z_{14}]\!] \\ \vdots & & \vdots \\ & \ddots & \\ [\![Z_{41}]\!] & \cdots & [\![Z_{44}]\!] \end{bmatrix} \cdot \begin{bmatrix} [\![J_z]\!] \\ [\![J_t]\!] \\ [\![M_z]\!] \\ [\![M_t]\!] \end{bmatrix} = [\,0\,] \tag{4.23}$$

or, by definition,

$$Z \cdot I = 0 \ . \tag{4.24}$$

In (4.23) each "element" $[\![Z_{mn}]\!]$ is an $N \times N$ matrix whose elements correspond to the appropriate terms in equations (4.18) – (4.19). Each current "element" in (4.23) represents an $N \times 1$ matrix whose elements are the unknown expansion coefficients of the corresponding current (see Eqs. 4.13 and 4.14).

To have a non-trivial solution to (4.23) we require that the determinant of the Z matrix vanish. Because of the approximate nature of the numerical implementation, a true zero of $|Z|$ may not exist. Rather, the "zeros" of $|Z|$ may only be local minima. To search for the minima we proceed as follows: given a particular waveguide geometry and the properties of the dielectric and conductor, we choose a value for the propagation constant k_z. Next, the elements of $[\![Z_{mn}]\!]$ are computed, followed by the computation of $|Z|$. We then vary k_z in the complex plane until a local minimum is found. The 2-dimensional search algorithm for k_z is based on the Powell's n-dimensional minimization routine [13,294].

In Chapter 2 we stated that our goal was to develop a procedure which could determine the allowed values of the propagation constant k_z for a waveguide structure. We now have that technique. Any k_z satisfying Maxwell's equations causes a minimum in $|Z|$. Finding all the allowable propagation constants is usually not required. For any practical waveguide of sufficient length, the behavior of a signal travelling along the guide is primarily influenced by the "propagating modes". These modes are characterized by a propagation constant having a finite and positive real part (the other modes are generally characterized by a purely imaginary propagation constant). Thus, we can instruct the search algorithm to minimize $|Z|$ by varying k_z along the real axis. Once a minimum is found along the real axis, we locally vary k_z in the complex plane until a local minimum is found.

4.4 Summary

In this chapter we introduced an approximate technique that may be used to solve integral equations. This technique, called the Method of Moments (MOM), reduces the integral equations to a set simultaneous linear equations, which may then be solved by a number of well-known algorithms. Using this technique we developed a computer based algorithm to solve the waveguide problem. In the next chapter we present results for various waveguides.

Chapter 5

Computer Program Results

5.1 Introduction

In this chapter we present the results of a computer program solution to the waveguide problem developed in Chapters 3 and 4. We first present the results for lossless rectangular and circular waveguides (Figs. 5.1 and 5.2). For these ideal cases, the propagation constant is known exactly [1]. By comparing the results with the theoretical values, we may estimate the validity and accuracy of the computer code. As an additional verification, the results for a ridged waveguide (Fig. 5.3) are compared with the approximations given by other authors (an exact solution is not known for the ridged waveguide). We conclude the chapter by presenting results for a lossy rectangular waveguide. The results are evaluated by comparing them with the estimations provided by perturbation theory.

5.2 Lossless Rectangular Waveguide

The first case we consider is the lossless $2 \times 1\,\mathrm{cm}$ rectangular waveguide (Fig. 5.1). For the cases studied in this section, we assume the dielectrics are air and the conductors are ideal. In addition, all the materials are assumed to be nonmagnetic, $\mu_c^* = \mu_d^* = \mu_o$ (we shall enforce the nonmagnetic condition in <u>all</u> the remaining problems in the thesis). For future reference, we define the propagation constant as

$$k_z = \beta - j\alpha \tag{5.1}$$

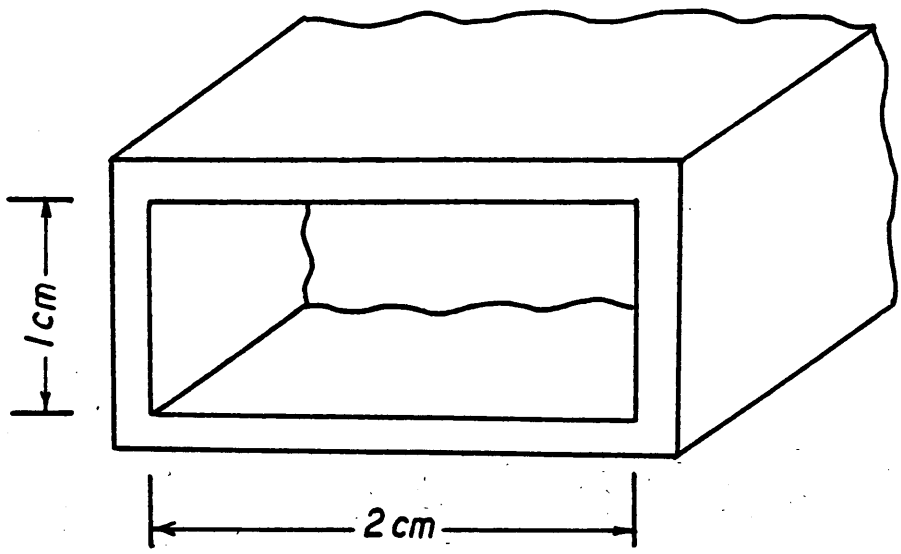

Figure 5.1. 2×1 cm rectangular waveguide.

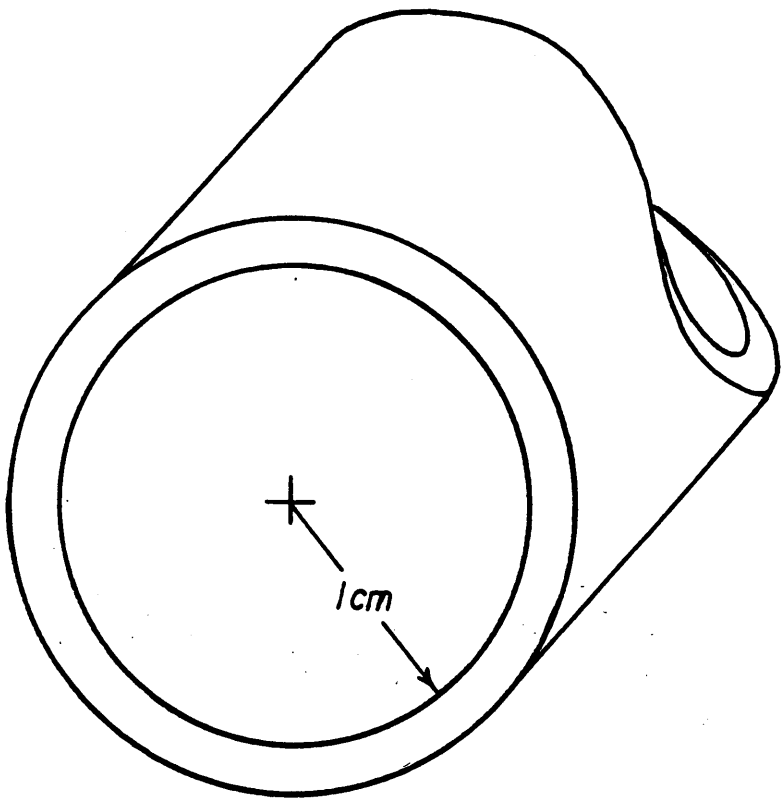

Figure 5.2. 1cm circular waveguide.

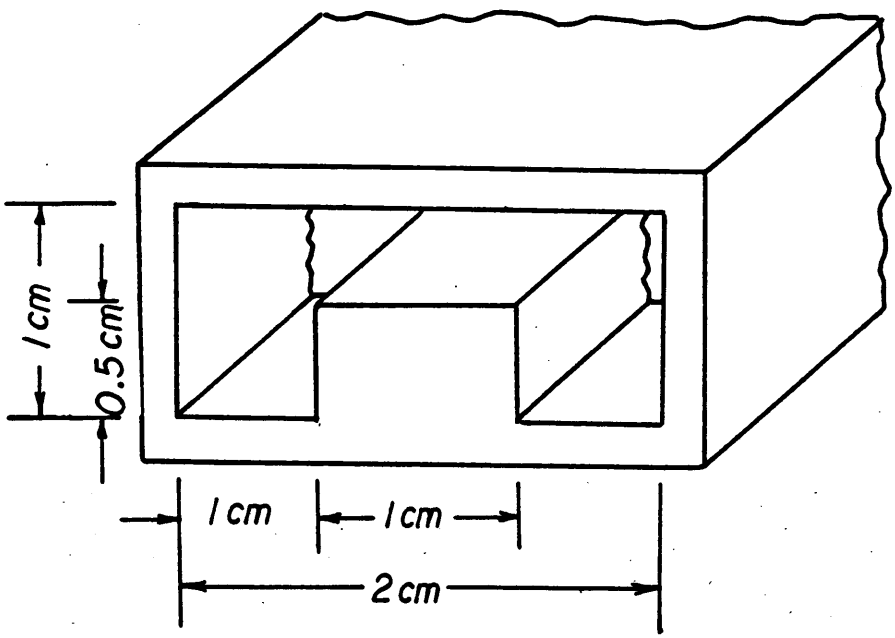

Figure 5.3. Ridged waveguide.

where β is called the phase constant and α is called the attenuation constant.

In Chapter 4 we noted that allowable values of the propagation constant (k_z) cause minima in the determinant of the matrix [Z]. This property is illustrated by in Fig. 5.4. The data was obtained using an operating frequency of 20 GHz, an attenuation constant of $\alpha = 0$, and a twelve point (N=12) approximation of the waveguide boundary. The ideal conductors were simulated by setting the conductivity to $\sigma = 1 \times 10^{30}$ S/m, a huge value. In Table 5.1 we compare the estimated values of k_z with the theoretical values for the TE_{10}, TE_{01}, TE_{20}, TE_{11}, and TM_{11} modes [1,150] (the estimated values are those at the minimums in Fig. 5.4). We note that the program accurately estimates the propagation constant for each mode. However, the minimum corresponding to the TE_{01} and TE_{20} modes (the second minimum in Fig. 5.4) is not as sharp or deep as the other two. A possible explanation is discussed below.

As mentioned above, the waveguide boundary was approximated using twelve points (Fig. 5.5). Examining the current distrubutions for the TE_{01} mode, one finds that the program is attempting to approximate a half-sine wave with three points (the three points on either side — Fig. 5.5). For the TE_{20} mode, we are attempting to approximate a full-sine wave with the five points located on either the top or bottom (Fig. 5.5). We propose that the current approximations are too coarse. To justify the explanation, the data was recomputed using two additional points on each side. The effect of the two new points should be a more accurate approximation to the TE_{01} currents. As expected, the minimum is now sharp and well defined (Fig. 5.6).

Returning to the original problem (N = 12), we change the operating frequency from f = 20 GHz to f = 5 GHz. At the new frequency the modes listed in Table 5.1 are cut-off, and the propagation constant becomes purely imaginary [1,384]. The results given in

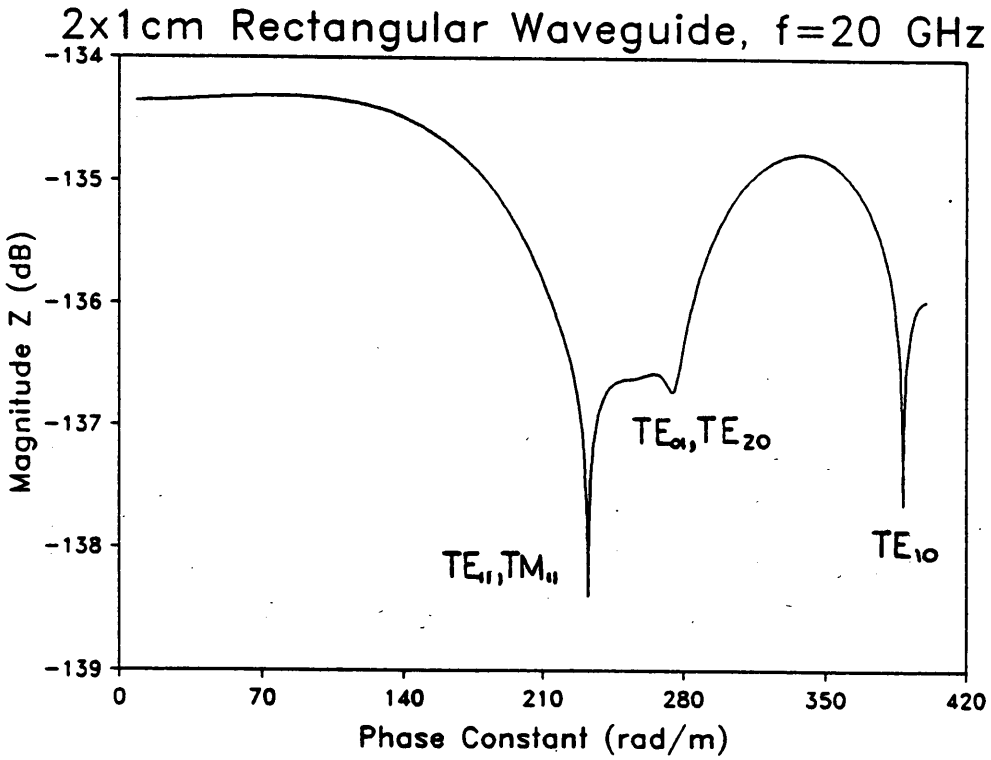

Figure 5.4. Plot of |Z| versus phase constant in a lossless 2×1 cm rectangular waveguide with $\epsilon_d^* = \epsilon_0$, $\sigma = 1 \times 10^{30}$ S/m, f = 20 GHz, and N = 12.

Table 5.1. 2×1 cm rectangular waveguide, f = 20 GHz
N = 12, $\sigma = 1 \times 10^{30}$ S/m, $\epsilon_d^* = \epsilon_0$,

	Phase Constant β (rad/m)		
Mode	Program	Theoretical	% Difference
TE_{10}	387.8	388.6	0.2
TE_{01} , TE_{20}	274.5	277.5	1.1
TE_{11} , TM_{11}	232.8	228.7	1.8

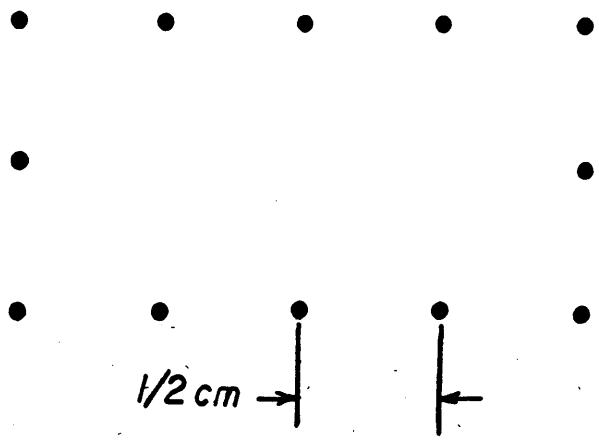

Figure 5.5. Discretization of rectangular waveguide for N = 12.

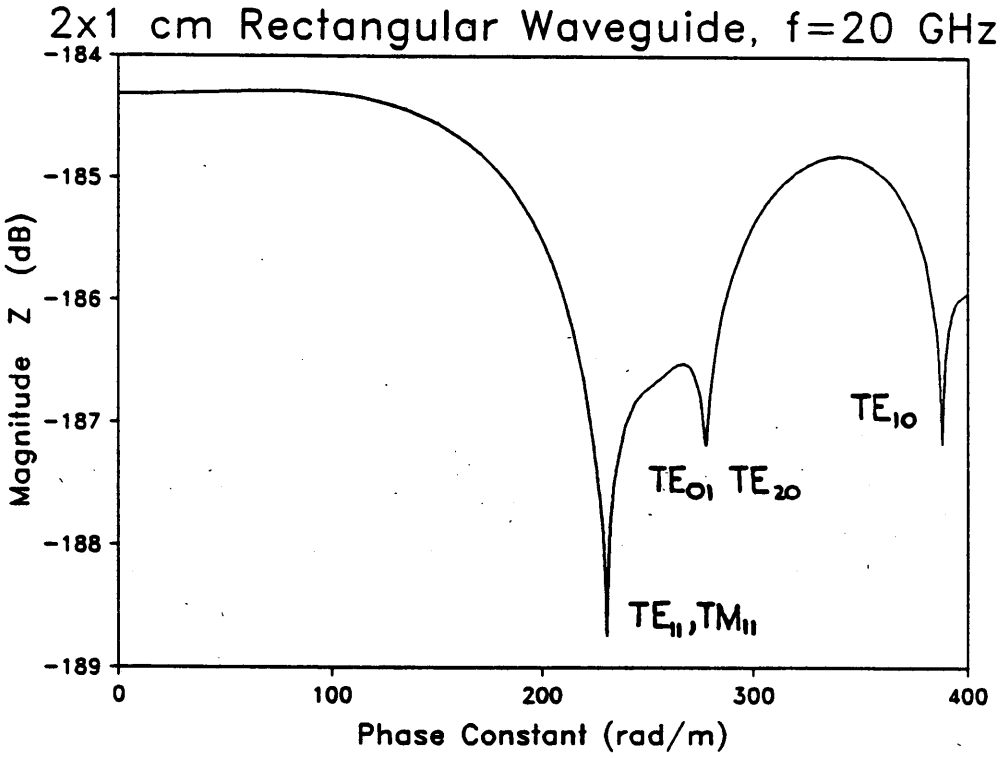

Figure 5.6. Plot of |Z| versus phase constant in a lossless 2×1 cm rectangular waveguide with $\epsilon_d^* = \epsilon_0$, $\sigma = 1 \times 10^{30}$ S/m, f = 20 GHz, and N = 16.

Fig. 5.7 and Table 5.2 demonstrate this property. As explained above, the shallow minimum shown in Fig. 5.7 corresponds to the TE_{01} and TE_{20} modes.

5.3 Lossless Circular Waveguide

Next, we consider the 1 cm (radius) waveguide depicted in Fig. 5.2. For the first case we let the boundary be approximated by $N = 12$ points, and choose an operating frequency of $f = 15$ GHz. At this frequency the modes TE_{11}, TM_{01}, and TE_{21} propagate. The variation of |Z| versus the phase constant is shown in Fig. 5.8. From the Fig. and Table 5.3 we see that the TE_{11} and TM_{01} modes are accurately predicted. However, the minimum in Fig. 5.8 corresponding to the TE_{21} mode is virtually unresolvable (the minimum should lie near $k_z = 74.6$ rad/m). Apparently, the number of points (12) is inadequate for this mode. If we increase the number of points to $N = 24$, we obtain the results given in Fig. 5.9 and Table 5.4. From Fig. 5.9 we note the minimum corresponding to the TE_{21} mode is now clearly visible. However, the broad, shallow, and erroneous location of this minimum suggests that even twenty-four points are insufficient. Predictably, the estimated propagation constant for the TE_{11} and TM_{01} modes have also been improved. This example has demonstrated a not-too-surprising result. Namely, by increasing the number of points, we increase the accuracy of the program. The increased accuracy is a direct result of the moment method technique. In Chapter 4 we noted, theoretically, that the method of moments solution becomes exact as the number of points approaches infinity (assuming a complete solution). However, if too many points are used in a computer solution, round-off error may become significant.

In Appendix C we approximated the double integrals by assuming the argument of the Hankel function was constant within the limits of the inner integral (see C.21 and C.22). We now investigate the effect of this approximation. Consider the Hankel function argument given

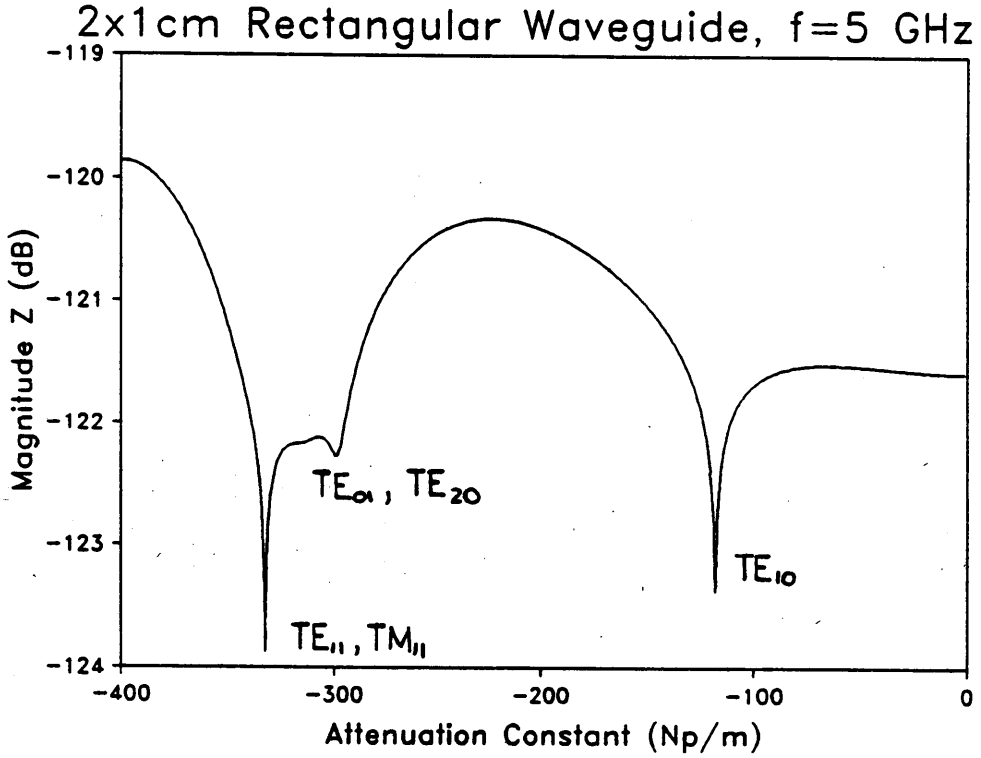

Figure 5.7. Plot of |Z| versus attenuatation constant in a 2×1 cm rectangular waveguide with $\epsilon_d^* = \epsilon_0$, $\sigma = 1 \times 10^{30}$ S/m, f = 5 GHz, and N = 12.

Table 5.2. 2×1 cm rectangular waveguide, f = 5 GHz
N = 12, $\sigma = 1 \times 10^{30}$ S/m, $\epsilon_d^* = \epsilon_0$,

	Attenuation Constant α (Np/m)		
Mode	Program	Theoretical	% Difference
TE_{10}	117.9	117.0	0.8
TE_{01} , TE_{20}	299.0	296.2	0.9
TE_{11} , TM_{11}	332.4	335.2	0.8

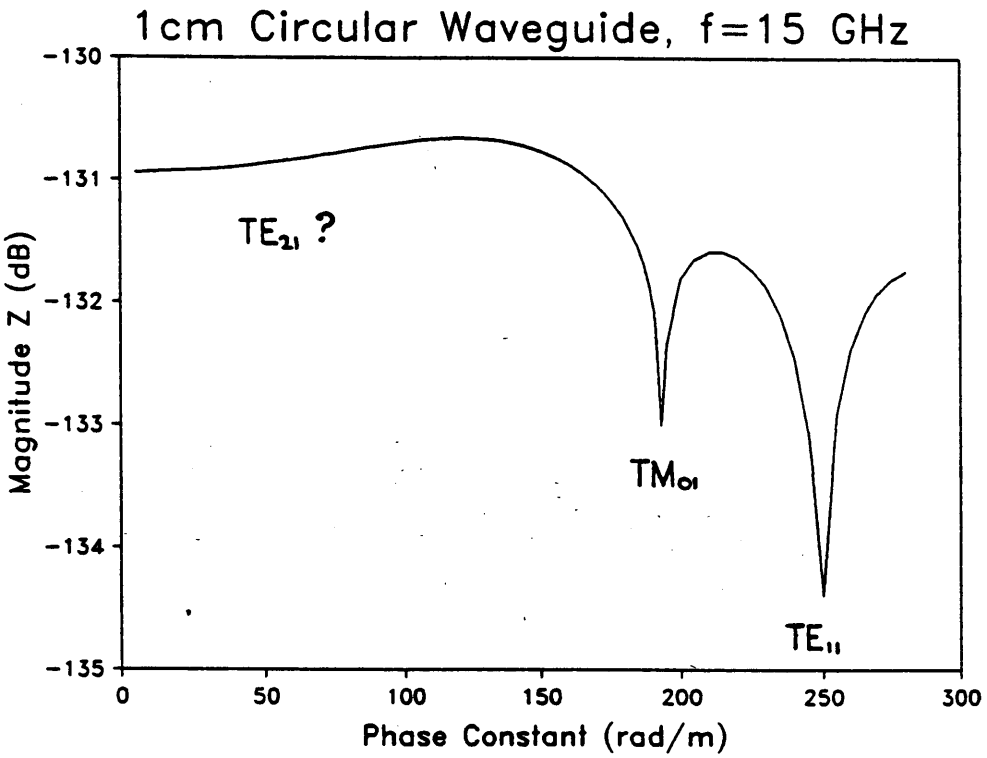

Figure 5.8. Plot of |Z| versus phase constant in a lossless 1 cm circular waveguide with $\epsilon_d^* = \epsilon_0$, $\sigma = 1 \times 10^{30}$ S/m, f = 15 GHz, and N = 12.

Table 5.3. 1 cm circular waveguide, f = 15 GHz

N = 12, $\sigma = 1 \times 10^{30}$ S/m, $\epsilon_d^* = \epsilon_0$,

	Phase Constant β (rad/m)		
Mode	Program	Theoretical	% Difference
TE_{11}	249.4	254.8	2.1
TM_{01}	193.4	202.5	4.5
TE_{21}	?	74.6	?

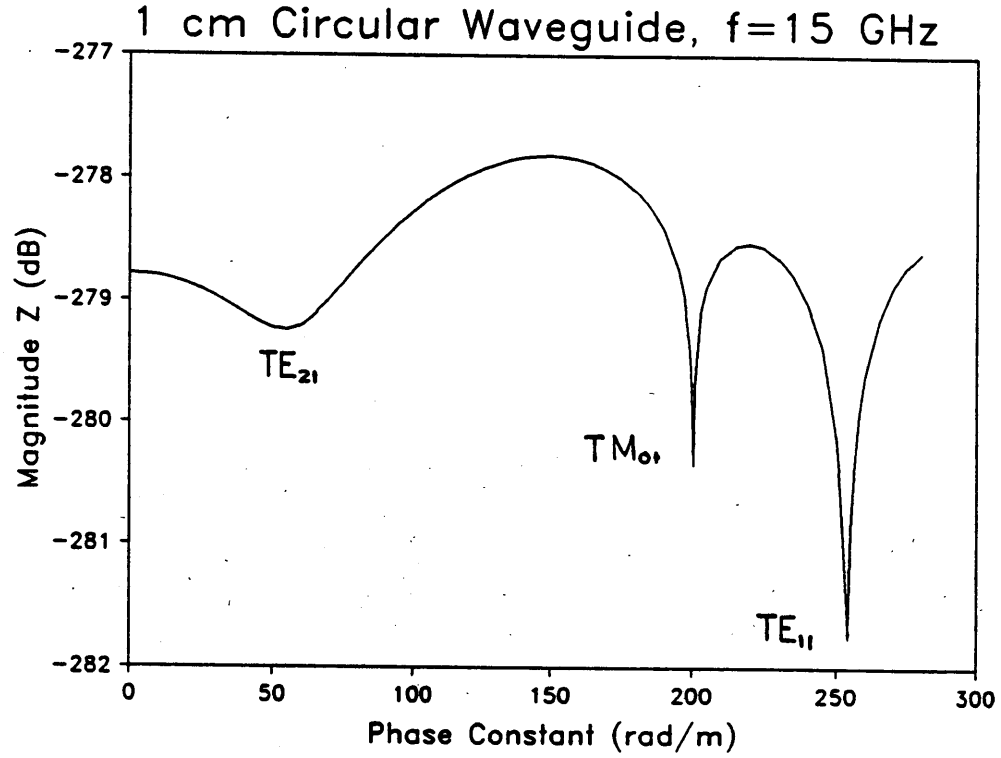

Figure 5.9. Plot of |Z| versus phase constant in a lossless 1 cm circular waveguide with $\epsilon_d^* = \epsilon_0$, $\sigma = 1 \times 10^{30}$ S/m, f = 15 GHz, and N = 24.

Table 5.4. 1 cm Circular Waveguide, f = 15 GHz
N = 24, $\sigma = 1 \times 10^{30}$ S/m, $\epsilon_d^* = \epsilon_0$,

	Phase Constant β (rad/m)		
Mode	Program	Theoretical	% Difference
TE_{11}	254.0	254.8	0.3
TM_{01}	200.5	202.5	1.0
TE_{21}	55	74.6	26.3

by equation (3.7),

$$\text{argument} = \sqrt{k_d{}^2 - k_z{}^2}\,\left|\rho - \rho'\right|. \tag{5.2}$$

From (5.2) we have

$$\frac{\partial(\text{argument})}{\partial\left|\rho - \rho'\right|} = \sqrt{k_d{}^2 - k_z{}^2}. \tag{5.3}$$

As the frequency increases in a lossless waveguide, the propagation constant (k_z) approaches the medium's intrinsic propagation constant (k_d) [1,384]. The result is that (5.3) becomes smaller and our approximations to the double integrals become better.

In Table 5.5 we demonstrate the effect of frequency on the program. The estimated phase constants correspond to the TE_{11} mode in a lossless circular waveguide. From the table we note the accuracy improves substantially with an increase in the operating frequency.

5.4 Lossless Ridged Waveguide

An additional verification of the program was obtained by considering the ridged waveguide shown in Fig. 5.3. An exact expression for the phase constant in this waveguide is not known. For this reason, we evaluate our results by comparing with approximations given by other authors.

For the present case, we choose an operating frequency of $f = 15\,GHz$ and approximate the boundary with $N = 20$ points. The resulting plot is shown in Fig. 5.10. From the estimated phase constants (minimum locations) we may compute the corresponding cut-off frequecies [1,384]. In Table 5.6 the estimated cut-off frequencies are compared with those given by [7,583].

Table 5.5. 1 cm Circular Waveguide, TE_{11} mode
$N = 12$, $\sigma = 1 \times 10^{30}$ S/m, $\epsilon_d^* = \epsilon_0$,

	Phase Constant β (rad/m)		
Frequency (GHz)	Program	Theoretical	% Difference
10	85.4	100.2	14.8
15	249.4	254.8	2.1
20	372.9	376.3	0.9

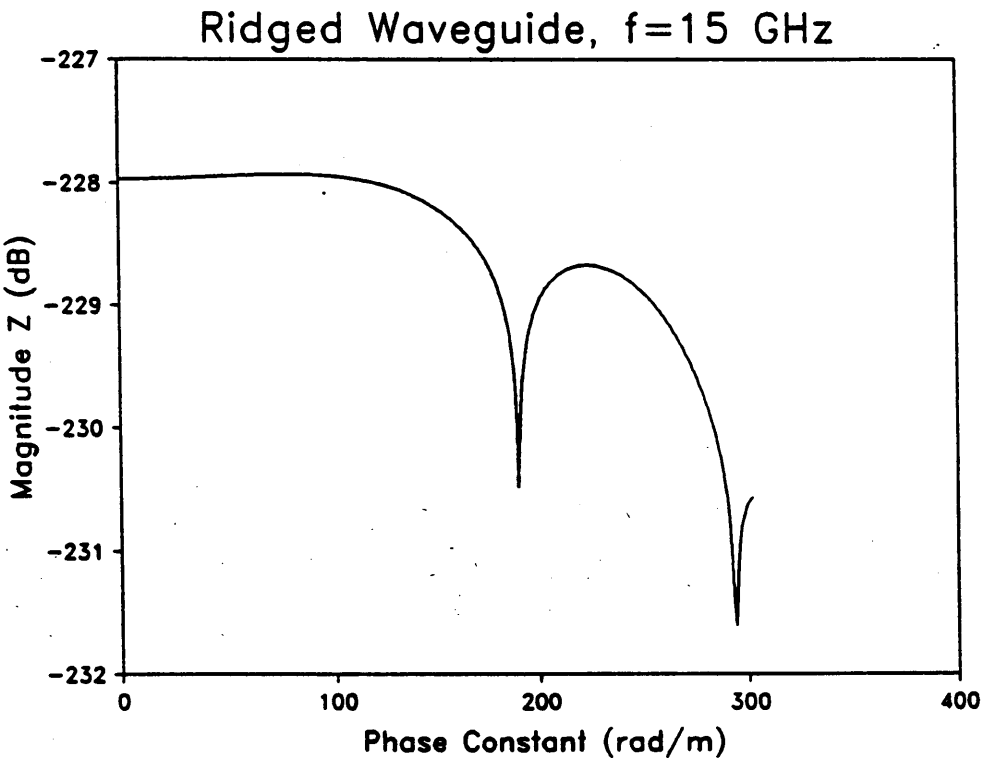

Figure 5.10. Plot of |Z| versus phase constant in a lossless ridged waveguide with $\epsilon_d^* = \epsilon_0$, $\sigma = 1 \times 10^{30}$ S/m, f = 15 GHz, and N = 20.

Table 5.6. Ridged Waveguide (Fig. 5.3), f=15 GHz
N = 20, $\sigma = 1 \times 10^{30}$ S/m, $\epsilon_d^* = \epsilon_0$,

	Cut-off Frequency (GHz)		
Mode	Program	Reference	% Difference
TE^{odd}	5.31	5.38	1.3
TE^{even}	11.95	11.78	1.4

5.5 Lossy Rectangular Waveguide

In this section loss is introduced into the rectangular waveguide problem depicted in Fig. 5.1. The loss may result from conductor and/or dielectric materials. In this section we treat each type of loss separately, and concentrate only on the loss associated with the TE_{10} mode.

The first problem we consider assumes the dielectric is air, the operating frequency is $f = 10$ GHz, and the boundary is approximated by $N = 12$ points. Three different conductivities were used, $\sigma = 1 \times 10^{30}$ S/m, $\sigma = 1 \times 10^{7}$ S/m, and $\sigma = 1 \times 10^{6}$ S/m. Recall in section 5.2 we simulated the lossless case by setting the conductivity to $\sigma = 1 \times 10^{30}$ S/m. We repeat this case because in section 5.2 we were not looking for any loss, and only the real part of k_z (β) was used to minimize the determinant |Z|. We now desire to minimize |Z| using both the real and imaginary parts of k_z.

The results are shown in Table 5.7. For all three conductivities the estimated attenuation constant grossly exceeds the values given by perturbation theory [1,71]. If the attenuation constant of the "lossless" case ($\sigma = 1 \times 10^{30}$ S/m) is subtracted from the "lossy" cases ($\sigma = 1 \times 10^{7}$ S/m , and $\sigma = 1 \times 10^{6}$ S/m), the results become much more reasonable (see the last column in Table 5.7). We now attempt to justify the subtraction scheme.

For a conductivity of $\sigma = 1 \times 10^{30}$ S/m the program should provide a vanishing attenuation constant. The predicted "loss" at this conductivity may be an inherent loss associtated with the discretization of the problem. For example, the loss may be viewed as a "radiation" through the finite grid used to approximate the boundary; Although, we do not claim the inherent loss is a radiation phenomenon, the analogy is provided as a convenient way to view the loss. For a sufficiently small "radiation" loss, the overall attenuation constant

Table 5.7. 2×1 cm Rectangular Waveguide, f = 10 GHz

TE_{10} mode, N = 12, $\epsilon_d^* = \epsilon_0$,

	Propagation Constant k_z (m^{-1})		
σ (S/m)	Program	Perturb. Theory	*
1×10^{30}	$137.95 - j0.2155$	$138.74 - j0.0$	$137.95 - j0.0$
1×10^{7}	$137.95 - j0.2424$	$138.74 - j0.0393$	$137.95 - j0.027$
1×10^{6}	$138.00 - j0.3010$	$138.74 - j0.1240$	$138.00 - j0.086$

* estimated k_z obtained by extracting the attenuation constant of the "lossless" case, $\sigma = 1 \times 10^{30}$ S/m.

should be given by

$$\alpha = \alpha_r + \alpha_{other} \tag{5.4}$$

where α_r is the attenuation constant due to the "radiation effect" and α_{other} is the attenuation constant due to other effects (e.g. finite conductivity). The above concept is the same technique where conductor and dielectric losses are added in a low-loss waveguide [1,74].

If we double the number of points in the current problem, we obtain the data given in Table 5.8. As expected, the computed propagation constants were improved (see the second column in Table 5.8). In particular, we note the attenuation constant corresponding to $\sigma = 1 \times 10^{30}$ S/m has been dramatically reduced. Since the grid is more closely spaced, we expect a reduced "radiation" effect. By comparing Tables 5.7 and 5.8 we observe an interesting feature — the "radiation-free" data (columns marked by $*$) are nearly the same in both cases. This feature tends to validate the subtraction scheme (equation 5.4).

In section 5.3 we noted the performance of the program should improve as the frequency is increased. We demonstrated this feature by showing the improvement of the phase constant in the circular waveguide. We now demonstrate the improvement in the attenuation constant. Consider the same problem used to generate Table 5.7. If the frequency is increased to $f = 20$ GHz, we obtain the data listed in Table 5.9. From the table we note the "radiation-free" propagation constants are now very close to the predictions given by perturbation theory.

We conclude this section by investigating dielectric loss. The problem we consider has the following parameters: $N = 12$, $f = 10$ GHz, and $\sigma = 1 \times 10^{30}$ S/m. The dielectric

Table 5.8. 2×1 cm Rectangular Waveguide, f = 10 GHz

TE_{10} mode, N = 24, $\epsilon_d^* = \epsilon_0$,

	Propagation Constant k_z (m^{-1})		
σ (S/m)	Program	Perturb. Theory	*
1×10^{30}	$138.68 - j0.0745$	$138.74 - j0.0$	$138.68 - j0.0$
1×10^{7}	$138.70 - j0.1010$	$138.74 - j0.0393$	$138.70 - j0.027$
1×10^{6}	$138.75 - j0.1596$	$138.74 - j0.1240$	$138.00 - j0.085$

* estimated k_z obtained by extracting the attenuation constant of the "lossless" case, $\sigma = 1 \times 10^{30}$ S/m.

Table 5.9. 2×1 cm Rectangular Waveguide, f = 20 GHz

TE_{10} mode, N = 12, $\epsilon_d^* = \epsilon_0$,

	Propagation Constant k_z (m^{-1})		
σ (S/m)	Program	Perturb. Theory	*
1×10^{30}	388.3 − *j*0.0766	388.6 − *j*0.0000	388.3 − *j*0.0000
1×10^{7}	388.4 − *j*0.1050	388.6 − *j*0.0290	388.4 − *j*0.0284
1×10^{6}	388,4 − *j*0.1675	388.6 − *j*0.0917	388.4 − *j*0.0909

* estimated k_z obtained by extracting the attenuation constant of the "lossless" case, $\sigma = 1 \times 10^{30}$ S/m.

constant is chosen to be,

$$\epsilon_d^* = \epsilon_0(1 - j\tan\delta) \tag{5.5}$$

where $\tan\delta$ is the loss tangent. In Table 5.10 we present TE_{10} loss data for several values of $\tan\delta$. From the "radiation-free" data in Table 5.10 we note the program accuractely estimates dielectric losses.

5.6 Summary

In this chapter computer program results were presented for three waveguides — the rectangular, circular, and ridged waveguides. We initially verified the code by comparing the computed results with the theoretical values for the lossless cases. Losses were then introduced by considering a rectanglar waveguide having imperfect conductors and a lossy dielectric. Investigation of the data led to a couple of important conclusions. First, we noted the program's accuracy improved as the frequency increased. This fact is a direct result of the approximations used in Appendix C. Second, the program appeared to have an inherent loss associated with the discretization of problem. Specifically, we found that the loss estimates were accurate provided that the apparent loss of the "lossless case" was properly taken into account.

Table 5.10. 2×1 cm Rectangular Waveguide, f = 10 GHz
TE_{10} mode, N = 12, $\epsilon_d^* = \epsilon_0(1 - j\tan\delta)$, $\sigma = 1\times10^{30}$ S/m

	Propagation Constant k_z (m^{-1})		
$\tan\delta$	Program	Theoretical	*
0	$137.95 - j0.216$	$138.74 - j0.0000$	$137.95 - j0.000$
0.001	$137.95 - j0.375$	$138.74 - j0.1583$	$137.95 - j0.159$
0.01	$137.96 - j1.807$	$138.75 - j1.5830$	$137.96 - j1.591$
0.1	$138.83 - j15.61$	$139.63 - j15.730$	$138.83 - j15.39$

* estimated k_z obtained by extracting the attenuation constant of the "lossless" case, $\sigma = 1 \times 10^{30}$ S/m.

Chapter 6

Summary and Conclusions

In this thesis a method has been presented which predicts the propagation constant in microwave guiding structures. The method is valid for guides having an arbitrary cross-section. In addition, both conductor and dielectric losses are included in the development.

The problem was formulated using integral representations of the fields in terms of vector potentials of the surface currents. The fields were evaluate at the boundaries separating the various regions (e.g. the dieltric and conductor regions). By imposing the continuity of tangential field components at the boundary, a set of coupled integral equations was derived.

The method of moments was used to reduce the set of coupled integral equations to a linear matrix equation. The resulting equation had the form

$$[Z] \cdot [I] = [0] \tag{6.1}$$

where $[I]$ represented the amplitudes of the unknown currents and $[Z]$ represented a "constant" matrix which depended on the propagation constant k_z (see Chapter 4).

To provide a nontrivial solution to (6.1), the propagation constant k_z was varied (for a given geometry) until a minimum of $|Z|$ was found. The computations were carried out using a computer program, and results were presented for three waveguide types — the rectangular, circular, and ridged waveguides. The program's ability to predict the propagation constant in both lossless and lossy waveguides was demonstrated.

Analysis of the program data led to several interesting points. First, not too surprisingly, the estimated propagation constant improved when the number of boundary points was increased. The method of moments directly predicts this result (see chapter 4). Second, increasing the frequency improved the program's accuracy. This feature was a result of certain approximations used in Appendix C. Finally, an inherent "radiation" loss associated with the discrete nature of the moment method was observed. Even under a simulated lossless condition ($\sigma = 1\times10^{30}$ S/m), the program predicted a finite attenuation constant. When the coductivity was set to reasonable values (e.g. 1×10^{7} S/m), the program overestimated the loss. However, once the "radiation loss" was extracted, the results were close to those given by perturbation theory.

Presently, several extensions of the work are under consideration. First, an "impedance boundary condition" type formulation is being considered. With this type of formulation, the resulting computations and matricies are simpler. A second possiblity is extending the program to allow for multi-layered dielectric/conductor geometries. Finally, inclusion of random, rough conducting surfaces is being considered as a possible dissertation topic.

References

[1] Harrington, R. F., *Time-Harmonic Electromagnetic Fields*, McGraw-Hill Book Company, New York, 1961.

[2] Gradshteyn, I. S., and I. M. Ryzhik, *Table of Integrals, Series, and Products*, Academic Press Inc., Orlando, 1980.

[3] Spiegel, M. R., *Vector Analysis*, Schaum's Outline Series, McGraw-Hill Book Company, New York, 1959.

[4] Spiegel, M. R., *Mathematical Handbook*, Schaum's Outline Series, McGraw-Hill Book Company, New York, 1968.

[5] Stutzman, W. L., and Gary A. Thiele, *Antenna Theory and Design*, John Wiley and Sons, New York, 1981.

[6] Van Bladel, J. , *Electromagnetic Fields*, McGraw-Hill, New York, 1964.

[7] Harrington R. F., and B. E. Spielman, "Waveguides of Arbitrary Cross Section by Solution of a Nonlinear Integral Eigenvalue Equation," *IEEE Transactions on Microwave Theory and Techniques*, Vol. MTT-20, September 1972.

[8] Fukai, I., and S. Kagami, "Application of Boundary-Element Method to Electromagnetic Field Problems," *IEEE Transactions on Microwave Theory and Techniques*, Vol. MTT-32, April 1984.

[9] Davies, J. B., and D. M. Syahkal, "Accurate Solution of Microstrip and Coplanar Structures for Dispersion and for Dielectric and Conductor Losses," *IEEE Transactions on Microwave Theory and Techniques*, Vol. MTT-27, July 1979.

[10] Mittra, R. (ed.), *Computer Techniques for Electromagnetics*, Hemisphere Publishing Corp., Washington, 1987.

[11] Taylor, A. E., and R. Mann, *Advanced Calculus*, John Wiley and Sons, Inc., New York, 1983.

[12] Harrington, R. F., *Field Computation by Moment Methods*, Macmillan, New York, 1968.

[13] Press, W. H. , et. al, *Numerical Recipes, The Art of Scientific Computing*, Cambridge University Press, New York, 1986.

[14] Mason, J. P., "Cylindrical Bessel Functions for a Large Range of Complex Arguments," *Computer Physics Communications*, Vol. 30, January 1983.

[15] Davis, W. A., "A Guide to Choosing Basis and Testing Functions in the Method of Moments," 1975 URSI Radio Science Meeting, Urbana, Ill, 3-5 June 1975.

[16] Collin, R. E., *Antennas and Radiowave Propagation*, McGraw-Hill Book Company, New York, 1985.

Appendix A

Derivation of Vector Potential Representations

Consider electromagnetic fields which exist in a homogeneous, isotropic region having a complex permitivity $\epsilon^*$and a complex permeability μ^*. Since Maxwell's equations are linear, the electromagnetic fields may be expressed as the sum of two fields — one field due to the electric sources J and the other field due to the magnetic sources M. If we define

$$\mathbf{E} \equiv \mathbf{E}^{\mathrm{e}} + \mathbf{E}^{\mathrm{m}} \tag{A.1}$$

$$\mathbf{H} \equiv \mathbf{H}^{\mathrm{e}} + \mathbf{E}^{\mathrm{m}} \tag{A.2}$$

and let the e fields be due to J and the m fields be due M, then we have [1,99]

$$-\nabla \times \mathbf{E}^{\mathrm{e}} = j\omega\mu^* \mathbf{H}^{\mathrm{e}} \tag{A.3}$$

$$\nabla \times \mathbf{H}^{\mathrm{e}} = j\omega\epsilon^* \mathbf{E}^{\mathrm{e}} + \mathbf{J} \tag{A.4}$$

$$-\nabla \times \mathbf{E}^{\mathrm{m}} = j\omega\mu^* \mathbf{H}^{\mathrm{m}} + \mathbf{M} \tag{A.5}$$

$$\nabla \times \mathbf{H}^{\mathrm{m}} = j\omega\epsilon^* \mathbf{E}^{\mathrm{m}} . \tag{A.6}$$

Taking the divergence of (A.3) and using the identity $\nabla \cdot (\nabla \times \mathrm{C}) \equiv 0$, we have

$$-\nabla \cdot (\nabla \times \mathbf{E}^{\mathrm{e}}) \equiv 0 = j\omega\mu^* (\nabla \cdot \mathbf{H}^{\mathrm{e}}) \tag{A.7}$$

or,

$$\nabla \cdot \mathbf{H}^{\mathrm{e}} = 0 . \tag{A.8}$$

From the identity $\nabla \cdot (\nabla \times \mathrm{C}) \equiv 0$, we may define an auxillary vector quantity, the magnetic vector potential A, as

$$\mathbf{H}^{\mathrm{e}} = \nabla \times \mathbf{A} . \tag{A.9}$$

Using (A.9), equation (A.3) may now be expressed as

$$\nabla \times (\mathbf{E}^{\mathrm{e}} + j\omega\mu^* \mathbf{A}) = 0 . \tag{A.10}$$

In view of the identity $\nabla \times (\nabla \Phi) \equiv 0$, we may define an auxillary scalar function Φ^e (the scalar electric potential) in the following manner:

$$-\nabla \Phi^e = \mathbf{E}^e + j\omega\mu^* \mathbf{A} \,. \tag{A.11}$$

Upon substituting (A.9) into (A.4) and employing the identity

$$\nabla \times \nabla \times \mathbf{C} \equiv \nabla(\nabla \cdot \mathbf{C}) - \nabla^2 \mathbf{C} \,,$$

we obtain

$$\nabla(\nabla \cdot \mathbf{A}) - \nabla^2 \mathbf{A} = j\omega\epsilon^* \mathbf{E}^e + \mathbf{J} \,. \tag{A.12}$$

Using (A.11),

$$\nabla(\nabla \cdot \mathbf{A}) - \nabla^2 \mathbf{A} = j\omega\epsilon^* \Big(-\nabla \Phi^e - j\omega\mu^* \mathbf{A} \Big) + \mathbf{J} \,. \tag{A.13}$$

Since only the curl of **A** has been specified, we are free to chose its divergence. If we let

$$\nabla \cdot \mathbf{A} = -j\omega\epsilon^* \Phi^e \,, \tag{A.14}$$

then (A.13) becomes

$$\nabla^2 \mathbf{A} + k^2 \mathbf{A} = -\mathbf{J} \tag{A.15}$$

where $k^2 \equiv \omega^2 \mu^* \epsilon^*$. Substituting (A.15) into (A.12) yields,

$$\mathbf{E}^e = \frac{1}{j\omega\epsilon^*} \Big(\nabla(\nabla \cdot \mathbf{A}) + k^2 \mathbf{A} \Big) \,. \tag{A.16}$$

The m equations, (A.5) and (A.6), are duals of the e equations. Proceding in an analogous manner, we obtain

$$\mathbf{E}^m = -\nabla \times \mathbf{F} \tag{A.17}$$

$$\nabla^2 \mathbf{F} + k^2 \mathbf{F} = -\mathbf{M} \tag{A.18}$$

and

$$\mathbf{H}^{m} = \frac{1}{j\omega\mu^{*}}\Big(\nabla(\nabla\cdot\mathbf{F}) + k^{2}\mathbf{F}\Big). \tag{A.19}$$

To summarize, equations (A.1) and (A.2) become

$$\mathbf{E} = -\nabla\times\mathbf{F} + \frac{1}{j\omega\epsilon^{*}}\Big(\nabla(\nabla\cdot\mathbf{A}) + k^{2}\mathbf{A}\Big) \tag{A.20}$$

$$\mathbf{H} = \nabla\times\mathbf{A} + \frac{1}{j\omega\mu^{*}}\Big(\nabla(\nabla\cdot\mathbf{F}) + k^{2}\mathbf{F}\Big) \tag{A.21}$$

with

$$\nabla^{2}\mathbf{A} + k^{2}\mathbf{A} = -\mathbf{J} \tag{A.22}$$

$$\nabla^{2}\mathbf{F} + k^{2}\mathbf{F} = -\mathbf{M} \tag{A.23}$$

and $$k^{2} = \omega^{2}\mu^{*}\epsilon^{*}.$$

Appendix B

Evaluation of Singular Integrals

In this appendix we evaluate the integrals developed in Chapter 3 at their singular points. The first integral to be considered has the form

$$\lim_{\epsilon \to 0} \lim_{\delta \to 0} \int_{-\epsilon}^{+\epsilon} I(\rho') \frac{1}{j4} H_o^{(2)}(k_\rho^d |\rho - \rho'|) \, dt' . \tag{B.1}$$

If we assume the contour ℓ (see figure B.1) is locally planar, the source location may be expressed as

$$\rho' \approx t' \hat{\mathbf{t}}' . \tag{B.2}$$

The procedure in Chapter 3 also specified that the field point is to be placed at

$$\rho = +\delta \hat{\mathbf{n}} \tag{B.3}$$

From figure B.1 we note that the argument of the Hankel function may be expressed as,

$$k_\rho^d |\rho - \rho'| = k_\rho^d \sqrt{(n-n')^2 + (t-t')^2} \tag{B.4}$$

with

$$n = +\delta , \quad n' = t = 0 .$$

Thus, the integral (B.1) is equivalent to

$$\lim_{\epsilon \to 0} \lim_{\delta \to 0} \frac{1}{j4} \int_{-\epsilon}^{+\epsilon} I(t') \, H_o^{(2)}\Big(k_\rho^d \sqrt{\delta^2 + t'^2} \Big) \, dt' . \tag{B.5}$$

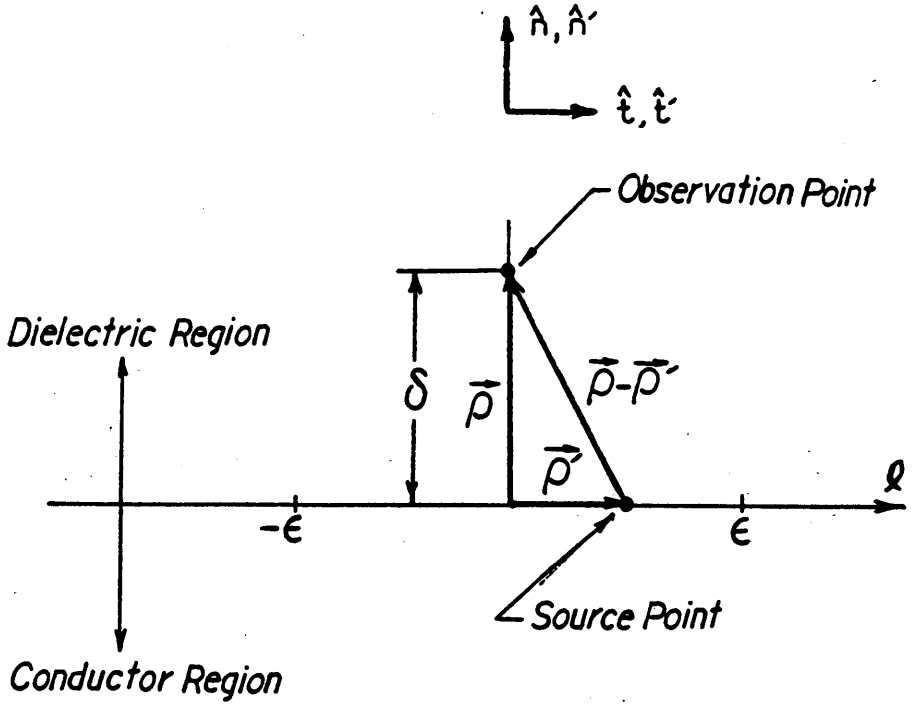

Figure B.1. Local geometry in the vicinity of the singular point

Given a sufficiently small argument, the series representation of the Green's function (see [2,951]) may be compactly written as

$$\frac{1}{j4} H_o^{(2)}\left(k_\rho \left|\rho-\rho'\right|\right) = -\frac{1}{2\pi}\left\{C + \ln\left(k_\rho^d \left|\rho-\rho'\right|\right) + O\left(\left|\rho-\rho'\right|^2 \ln\left|\rho-\rho'\right|\right)\right\} \tag{B.6}$$

where C represents a constant term and $O\left(\left|\rho-\rho'\right|^2 \ln\left|\rho-\rho'\right|\right)$ represents terms bounded by order of magnitude $\left|\rho-\rho'\right|^2 \ln\left|\rho-\rho'\right|$. The current may be expanded in a Taylor series about $t'=0$ giving [4,110]

$$I(t') = I(0) + t' \left.\frac{\partial I}{\partial t'}\right|_{t'=0} + \frac{1}{2!}(t')^2 \left.\frac{\partial^2 I}{(\partial t')^2}\right|_{t'=0} + \cdots . \tag{B.7}$$

If we assume that the current is sufficiently smooth within the interval 2ϵ, then (B.7) is equivalent to

$$I(t') = I(0) + O(t') , \tag{B.8}$$

and the integral (B.5) may be written as

$$\lim_{\epsilon \to 0} \lim_{\delta \to 0} -\frac{1}{2\pi} \int_{-\epsilon}^{+\epsilon} \left(I(0) + O(t')\right)\left(C + \ln\left(k_\rho^d \sqrt{\delta^2 + t'^2}\right) + O\left\{\left(\delta^2 + t'^2\right) \ln \sqrt{\delta^2 + t'^2}\right\}\right) dt' \tag{B.9}$$

where the conditions $n = +\delta$, and $n' = t = 0$ have been enforced. Expanding the integrand and using the $O(\cdot)$ notation, the integrand of (B.9) may be expressed as,

$$I(0)C + I(0)\ln\left(k_\rho^d \sqrt{\delta^2 + t'^2}\right) + O(t')\ln\left(k_\rho^d \sqrt{\delta^2 + t'^2}\right). \tag{B.10}$$

Obviously, the integral involving $I(0)C$ approachs zero as $\epsilon \rightarrow 0$. For sufficiently small arguments, the third term of (B.10) is bounded by

$$\left| O(t') \ln\left(k_\rho^d \sqrt{\delta^2 + t'^2} \right) \right| \leq \left| O(t') \ln\left(k_\rho^d |t'| \right) \right| . \tag{B.11}$$

As $\epsilon \rightarrow 0$ the right hand side of (B.11) behaves as

$$\left| O(\epsilon) \ln\left(k_\rho^d |t'| \right) \right| \sim \lim_{\epsilon \rightarrow 0} |\epsilon \ln(\epsilon)| = 0 . \tag{B.12}$$

Therefore, (B.9) may be evaluated by simply considering an integral of the form

$$\lim_{\epsilon \rightarrow 0} \lim_{\delta \rightarrow 0} -\frac{I(0)}{2\pi} \int_{-\epsilon}^{+\epsilon} \ln\left(k_\rho^d \sqrt{\delta^2 + t'^2} \right) dt' . \tag{B.13}$$

This integral may be directly integrated giving

$$\lim_{\epsilon \rightarrow 0} \lim_{\delta \rightarrow 0} -\frac{I(0)}{2\pi} \left(t' \ln\left(k_\rho^d \sqrt{\delta^2 + t'^2} \right) - 2t' + 2\delta \tan^{-1}\left(\frac{t'}{\delta} \right) \right) \Bigg|_{-\epsilon}^{+\epsilon} \tag{B.14}$$

or,

$$\lim_{\epsilon \rightarrow 0} -\frac{I(0)}{\pi} \left(\epsilon \ln(k_\rho^d |\epsilon|) - 2\epsilon \right) = 0 . \tag{B.15}$$

Therefore, the singular contribution of (B.1) is zero.

The next singular integral we need to consider is

$$\lim_{\epsilon \rightarrow 0} \lim_{\delta \rightarrow 0} \int_{-\epsilon}^{+\epsilon} I(\rho') \frac{1}{j4} \frac{\partial}{\partial n'} H_o^{(2)}(k_\rho^d |\rho - \rho'|) \, dt' . \tag{B.16}$$

By using (B.4), (B.6) and (B.8), integral (B.16) may be expressed as,

$$-\frac{1}{2\pi}\lim_{\epsilon\to 0}\lim_{\delta\to 0}\int_{-\epsilon}^{+\epsilon} I(0)\frac{\partial}{\partial n'}\Bigg(C+\ln\Big(k_\rho^d\sqrt{(n-n')^2+(t')^2}\Big)$$

$$+\,O\Big[\Big((n-n')^2+(t')^2\Big)\ln\Big(\sqrt{(n-n')^2+(t')^2}\Big)\Big]\Bigg)dt'\Bigg|_{n=+\delta,\,n'=0} \qquad \text{(B.17)}$$

which is equivalent to,

$$-\frac{1}{2\pi}I(0)\Bigg(\lim_{\epsilon\to 0}\lim_{\delta\to 0}\int_{-\epsilon}^{+\epsilon}\frac{-\delta}{\delta+(t')^2}\,dt'$$

$$+\lim_{\epsilon\to 0}\lim_{\delta\to 0}\int_{-\epsilon}^{+\epsilon}O\Big(\delta\ln\sqrt{\delta^2+(t')^2}\Big)\Bigg)dt'\,. \qquad \text{(B.18)}$$

Obviously, the second integral of (B.18) vanishes as $\delta\to 0$. Integrating the first term yields,

$$\frac{I(0)}{2\pi}\lim_{\epsilon\to 0}\lim_{\delta\to 0}\tan^{-1}\frac{t'}{\delta}\Bigg|_{-\epsilon}^{+\epsilon}=\frac{I(0)}{2\pi}\Big(\frac{\pi}{2}-\Big(-\frac{\pi}{2}\Big)\Big)=\frac{I(0)}{2}\,. \qquad \text{(B.19)}$$

Another integral that must be evaluated has the form,

$$\lim_{\epsilon\to 0}\lim_{\delta\to 0}\int_{-\epsilon}^{+\epsilon} I(\rho')\,\frac{1}{j4}\frac{\partial}{\partial n}H_o^{(2)}\big(k_\rho^d|\rho-\rho'|\big)\,dt'\,. \qquad \text{(B.20)}$$

The difference between (B.20) and (B.16) is the variable which is differentiated. The only consequence of the new derivative is a negative sign (see B.17). We conclude that (B.20) reduces to

$$-\frac{I(0)}{2}\,. \qquad \text{(B.21)}$$

The final integral we need to consider is

$$\lim_{\epsilon \to 0} \lim_{\delta \to 0} \frac{\partial}{\partial t} \int_{-\epsilon}^{+\epsilon} I(\rho') \, \frac{1}{j4} \, H_o^{(2)}\left(k_\rho^d \left| \rho - \rho' \right| \right) \, dt' \tag{B.22}$$

which, using (B.4), (B.6), and (B.8), is equivalent to

$$\lim_{\epsilon \to 0} \lim_{\delta \to 0} -\frac{1}{2\pi} \frac{\partial}{\partial t} \int_{-\epsilon}^{+\epsilon} \Big(I(0) + O(t') \Big) \Bigg(\mathrm{C} + \ln\Big(k_\rho^d \sqrt{\delta^2 + (t-t')^2} \Big)$$

$$+ O\Big\{ \Big(\delta^2 + (t-t')^2 \Big) \ln \sqrt{\delta^2 + (t-t')^2} \Big\} \Bigg) dt' \Bigg|_{t=0} . \tag{B.23}$$

Obviously, as $\epsilon \to 0$, the term involving $I(0)\mathrm{C}$ contributes nothing to the integral. Integrating the remaining terms yields,

$$\lim_{\epsilon \to 0} \lim_{\delta \to 0} I(0) \, \frac{\partial}{\partial t} \Bigg((t-t') \ln\Big(\sqrt{\delta^2 + (t-t')^2} \Big) + (t-t') - \delta \tan^{-1} \frac{(t-t')}{\delta} +$$

$$O\Big\{ t^2 \ln \sqrt{\delta^2 + (t-t')^2} \Big\} \Bigg) \Bigg|_{-\epsilon,\, t=0}^{+\epsilon} \tag{B.24}$$

Evaluating (B.24) at the limits of integration and taking the derivative gives,

$$I(0) \lim_{\epsilon \to 0} \lim_{\delta \to 0} \Bigg(\frac{-(\epsilon - t)^2}{\delta^2 + (t-\epsilon)^2} - \ln\Big(\sqrt{\delta^2 + (t-\epsilon)^2} \Big) + 1$$

$$- \frac{\delta^2}{\delta^2 + (t-\epsilon)^2} + \frac{(\epsilon + t)^2}{\delta^2 + (t+\epsilon)^2} + \ln\Big(\sqrt{\delta^2 + (t+\epsilon)^2} \Big)$$

$$- 1 + \frac{\delta^2}{\delta^2 + (t+\epsilon)^2} + O\Big\{ t \ln \sqrt{\delta^2 + (t-\epsilon)^2} \Big\} \Bigg) \Bigg|_{t=0} . \tag{B.25}$$

Once (B.25) is evaluated at $t = 0$, the first eight terms cancel and the last term is zero. We conclude that the integral given by (B.22) is zero.

Appendix C

Numerical Form Derivation

In Chapter 4 we found that our numerical formulation led to the following form of equation (3.41) — see equation (4.17):

$$\int_{t_m'}^{t_{m+1}'} \mathcal{F}(t)\ \delta\Big(t - t_m' - \frac{\Delta_m}{2}\Big)\ dt = 0,\ \ m = [1 \ldots N]\ . \tag{C.1}$$

where,

$$\mathcal{F}(t) \equiv \int_\ell \Big(\frac{\partial G^d}{\partial n'} + \frac{\partial G^c}{\partial n'}\Big) \sum_{n=1}^{N} M_n^t \left(1 - \frac{|t' - t_n'|}{\Delta}\right) P_{2n}(t')\ dt'$$

$$+ \int_\ell \left(\frac{{k_d}^2 - {k_z}^2}{j\omega\epsilon_d^*} G^d + \frac{{k_c}^2 - {k_z}^2}{j\omega\epsilon_c^*} G^c\right) \sum_{n=1}^{N} J_n^z P_n(t')\ dt'$$

$$-jk_z \int_\ell \left(\frac{1}{j\omega\epsilon_d^*} G^d + \frac{1}{j\omega\epsilon_c^*} G^c\right) \frac{\partial}{\partial t'} \sum_{n=1}^{N} J_n^t \left(1 - \frac{|t' - t_n'|}{\Delta}\right) P_{2n}(t')\, dt'. \tag{C.2}$$

The left hand side of (C.1) is equivalent to evaluating (C.2) with the field point located at the middle of segment $\Delta\ell_m$. If we use this fact along with the fact that the current amplitudes,

J_n^z, J_n^t, and M_n^t, are constants, then (C.1) may be written as

$$\sum_{n=1}^{N} M_n^t \int_\ell \left(\frac{\partial G^d}{\partial n'} + \frac{\partial G^c}{\partial n'} \right) \left(1 - \frac{|t' - t_n'|}{\Delta} \right) P_{2n}(t')\, dt'$$

$$+ \sum_{n=1}^{N} J_n^z \int_\ell \left(\frac{k_d^2 - k_z^2}{j\omega\epsilon_d^*} G^d + \frac{k_c^2 - k_z^2}{j\omega\epsilon_c^*} G^c \right) P_n(t')\, dt'$$

$$- j k_z \sum_{n=1}^{N} J_n^t \int_\ell \left(\frac{1}{j\omega\epsilon_d^*} G^d + \frac{1}{j\omega\epsilon_c^*} G^c \right) \frac{\partial}{\partial t'} \left(1 - \frac{|t' - t_n'|}{\Delta} \right) P_{2n}(t')\, dt' = 0 \qquad \text{(C.3)}$$

with $m = [1 \ldots N]$. Keep in mind that for a given m the field point is located at the midpoint of segment $\Delta\ell_m$.

Using the definition of $P_{2n}(t')$ (see equation 4.14), we may define the first integral in (C.3) as,

$$A_{mn}^d + A_{mn}^c \qquad \text{(C.4a)}$$

where,

$$A_{mn}^d \equiv \int_{t_{n-1}'}^{t_n'} \frac{\partial G^d}{\partial n'} \left(1 - \frac{t_n' - t'}{\Delta_{n-1}} \right) dt'$$

$$+ \int_{t_n'}^{t_{n+1}'} \frac{\partial G^d}{\partial n'} \left(1 - \frac{t' - t_n'}{\Delta_n} \right) dt' \qquad \text{(C.4b)}$$

and

$$A_{mn}^c \equiv \int_{t_{n-1}'}^{t_n'} \frac{\partial G^c}{\partial n'} \left(1 - \frac{t_n' - t'}{\Delta_{n-1}} \right) dt'$$

$$+ \int_{t_n'}^{t_{n+1}'} \frac{\partial G^c}{\partial n'} \left(1 - \frac{t' - t_n'}{\Delta_n} \right) dt' \; . \qquad \text{(C.4c)}$$

The subscript m in (C.4) reminds us that the observation point is located at the midpoint of the segment $\Delta\ell_m$. Since the observation point is fixed for a given m, $A_{mn}^d + A_{mn}^c$ may be evaluated via numerical integration. However, to numerically implement (C.4) in its present

form would require an approximation of the derivative terms (e.g. finite difference). Another approach (the author's choice) involves evaluating these derivates analytically. Consider the vector which defines the observation point with respect to the source point location $(\rho-\rho')$ — Fig. C.1. If we define ϕ as the the angle between the vector $(\rho-\rho')$ and $\hat{n}'$ (the normal at the source location), then from [5,369] we have

$$\frac{\partial G^d}{\partial n'} = \frac{k_\rho^d}{j4}\cos\phi\; H_1^{(2)}\left(k_\rho^d\;|\rho-\rho'|\right) \tag{C.5}$$

or,

$$\frac{\partial G^d}{\partial n'} = \frac{k_\rho^d}{j4}\left(\hat{R}\cdot\hat{n}'\right) H_1^{(2)}\left(k_\rho^d\;|\rho-\rho'|\right) \tag{C.6}$$

where,

$$\hat{R} \equiv \frac{\rho-\rho'}{|\rho-\rho'|}\ . \tag{C.7}$$

In a similar manner,

$$\frac{\partial G^c}{\partial n'} = \frac{k_\rho^c}{j4}\left(\hat{R}\cdot\hat{n}'\right) H_1^{(2)}\left(k_\rho^c\;|\rho-\rho'|\right)\ . \tag{C.8}$$

Now, consider the second integral of (C.3). From the definition of $P_n(t')$ this integral is equivalent to

$$\int_{t_n'}^{t_{n+1}'}\left(\frac{k_d^{\,2}-k_z^{\,2}}{j\omega\epsilon_d^*}G^d + \frac{k_c^{\,2}-k_z^{\,2}}{j\omega\epsilon_c^*}G^c\right)dt'\ . \tag{C.9}$$

We define

$$\mathbb{B}_{mn}^d \equiv \int_{t_n'}^{t_{n+1}'} G^d\; dt' \tag{C.10}$$

and

$$\mathbb{B}_{mn}^c \equiv \int_{t_n'}^{t_{n+1}'} G^c\; dt'\ . \tag{C.11}$$

Now, (C.9) may be written as

$$\left(\frac{k_d^{\,2}-k_z^{\,2}}{j\omega\epsilon_d^*}\right)\mathbb{B}_{mn}^d + \left(\frac{k_c^{\,2}-k_z^{\,2}}{j\omega\epsilon_c^*}\right)\mathbb{B}_{mn}^c\ . \tag{C.12}$$

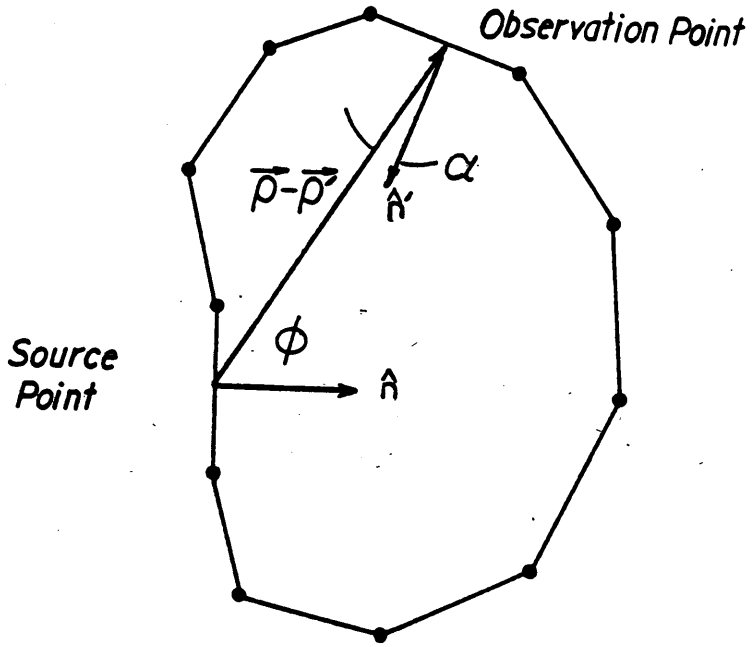

Figure C.1. Angles defining the relationship between the source and observation points.

From the definition of $P_{2n}(t')$ the third integral of (C.3) becomes

$$\int_{t'_{n-1}}^{t'_n} \left(\frac{1}{j\omega\epsilon_d^*} G^d + \frac{1}{j\omega\epsilon_c^*} G^c \right) \frac{\partial}{\partial t'} \left(1 - \frac{t'_n - t'}{\Delta_{n-1}} \right)$$

$$+ \int_{t'_n}^{t'_{n+1}} \left(\frac{1}{j\omega\epsilon_d^*} G^d + \frac{1}{j\omega\epsilon_c^*} G^c \right) \frac{\partial}{\partial t'} \left(1 - \frac{t' - t'_n}{\Delta_n} \right) dt' \qquad \text{(C.13)}$$

which is equivalent to

$$\frac{1}{j\omega\epsilon_d^*} C^d_{mn} + \frac{1}{j\omega\epsilon_c^*} C^c_{mn} \qquad \text{(C.14)}$$

where

$$C^d_{mn} \equiv \int_{t'_{n-1}}^{t'_n} \frac{1}{\Delta_{n-1}} G^d \, dt' - \int_{t'_n}^{t'_{n+1}} \frac{1}{\Delta_n} G^d \, dt' \qquad \text{(C.15a)}$$

and

$$C^c_{mn} \equiv \int_{t'_{n-1}}^{t'_n} \frac{1}{\Delta_{n-1}} G^c \, dt' - \int_{t'_n}^{t'_{n+1}} \frac{1}{\Delta_n} G^c \, dt' \; . \qquad \text{(C.15b)}$$

Using (C.4), (C.12), and (C.14), equation (C.3) may be expressed as

$$\sum_{n=1}^{N} M^t_n \left(\mathbb{A}^d_{mn} + \mathbb{A}^c_{mn} \right) + \sum_{n=1}^{N} J^z_n \left(\frac{k_d^2 - k_z^2}{j\omega\epsilon_d^*} \mathbb{B}^d_{mn} + \frac{k_c^2 - k_z^2}{j\omega\epsilon_c^*} \mathbb{B}^c_{mn} \right)$$

$$- j k_z \sum_{n=1}^{N} J^t_n \left(\frac{1}{j\omega\epsilon_d^*} C^d_{mn} + \frac{1}{j\omega\epsilon_c^*} C^c_{mn} \right) = 0 \;\; , \;\; m = [1 \ldots N] \, . \qquad \text{(C.16)}$$

If we substitute the current expansions (equations 4.13 and 4.14) into the integral equation (3.42) we obtain

$$
\begin{aligned}
&-jk_z \int_\ell \left(G^d + G^c\right) \sum_{n=1}^{N} M_n^t \left(1 - \frac{|t' - t_n'|}{\Delta}\right) P_{2n}(t') \, (\hat{n}' \cdot \hat{t}) \, dt' \\
&+ \int_\ell \left(\frac{\partial G^d}{\partial n} + \frac{\partial G^c}{\partial n}\right) \sum_{n=1}^{N} M_n^z P_n(t') \, dt' \\
&\frac{\partial}{\partial t} \int_\ell \left(\frac{1}{j\omega\epsilon_d^*} G^d + \frac{1}{j\omega\epsilon_c^*} G^c\right) \frac{\partial}{\partial t'} \sum_{n=1}^{N} J_n^t \left(1 - \frac{|t' - t_n'|}{\Delta}\right) P_{2n}(t') \, dt' \\
&-jk_z \frac{\partial}{\partial t} \int_\ell \left(\frac{1}{j\omega\epsilon_d^*} G^d + \frac{1}{j\omega\epsilon_c^*} G^c\right) \sum_{n=1}^{N} J_n^z P_n(t') \, dt' \\
&+ \int_\ell \left(\frac{k_d^2}{j\omega\epsilon_d^*} G^d + \frac{k_c^2}{j\omega\epsilon_c^*} G^c\right) \sum_{n=1}^{N} J_n^t \left(1 - \frac{|t' - t_n'|}{\Delta}\right) P_{2n}(t') \, (\hat{t}' \cdot \hat{t}) \, dt' = 0.
\end{aligned}
\tag{C.17}
$$

Multiplying (C.17) by the weight function (4.20) and integrating yields,

$$
\int_{t_{m-}'}^{t_{m+}'} \mathcal{G}(t) \, dt = 0, \quad m = [1 \ldots N] \tag{C.18}
$$

where $\mathcal{G}(t)$ is defined as

$$
\begin{aligned}
\mathcal{G}(t) \equiv &-jk_z \int_\ell \left(G^d + G^c\right) \sum_{n=1}^{N} M_n^t \left(1 - \frac{|t' - t_n'|}{\Delta}\right) P_{2n}(t') \, (\hat{n}' \cdot \hat{t}) \, dt' \\
&+ \int_\ell \left(\frac{\partial G^d}{\partial n} + \frac{\partial G^c}{\partial n}\right) \sum_{n=1}^{N} M_n^z P_n(t') \, dt' \\
&+ \frac{\partial}{\partial t} \int_\ell \left(\frac{1}{j\omega\epsilon_d^*} G^d + \frac{1}{j\omega\epsilon_c^*} G^c\right) \frac{\partial}{\partial t'} \sum_{n=1}^{N} J_n^t \left(1 - \frac{|t' - t_n'|}{\Delta}\right) P_{2n}(t') \, dt' \\
&-jk_z \frac{\partial}{\partial t} \int_\ell \left(\frac{1}{j\omega\epsilon_d^*} G^d + \frac{1}{j\omega\epsilon_c^*} G^c\right) \sum_{n=1}^{N} J_n^z P_n(t') \, dt' \\
&+ \int_\ell \left(\frac{k_d^2}{j\omega\epsilon_d^*} G^d + \frac{k_c^2}{j\omega\epsilon_c^*} G^c\right) \sum_{n=1}^{N} J_n^t \left(1 - \frac{|t' - t_n'|}{\Delta}\right) P_{2n}(t') \, (\hat{t}' \cdot \hat{t}) \, dt'.
\end{aligned}
\tag{C.19}
$$

Recall that in Chapter 4 we defined t'_{m-} and t'_{m+} as the midpoints of segments $\Delta\ell_{m-1}$ and $\Delta\ell_m$, respectively.

The first term of (C.18) is equivalent to

$$
\begin{aligned}
-jk_z \sum_{n=1}^{N} M_n^t \Bigg\{ & \int_{t'_{m-}}^{t'_m} \int_{t'_{n-1}}^{t'_n} \left(G^d + G^c\right)\left(1 - \frac{t'_n - t'}{\Delta_{n-1}}\right)(\hat{n}' \cdot \hat{t})\, dt'\, dt \\
& + \int_{t'_m}^{t'_{m+}} \int_{t'_{n-1}}^{t'_n} \left(G^d + G^c\right)\left(1 - \frac{t'_n - t'}{\Delta_{n-1}}\right)(\hat{n}' \cdot \hat{t})\, dt'\, dt \\
& + \int_{t'_{m-}}^{t'_m} \int_{t'_n}^{t'_{n+1}} \left(G^d + G^c\right)\left(1 - \frac{t' - t'_n}{\Delta_n}\right)(\hat{n}' \cdot \hat{t})\, dt'\, dt \\
& + \int_{t'_m}^{t'_{m+}} \int_{t'_n}^{t'_{n+1}} \left(G^d + G^c\right)\left(1 - \frac{t' - t'_n}{\Delta_n}\right)(\hat{n}' \cdot \hat{t})\, dt'\, dt \Bigg\}.
\end{aligned}
\tag{C.20}
$$

Since $\hat{t}$ and $\hat{n}'$ are constant within the limits of each double integral, the dot products may be taken outside the integrations. Interchanging the order of integration yields,

$$
\begin{aligned}
-jk_z \sum_{n=1}^{N} M_n^t \Bigg\{ & (\hat{n}'_{n-} \cdot \hat{t}_{m-}) \int_{t'_{n-1}}^{t'_n} \left(1 - \frac{t'_n - t'}{\Delta_{n-1}}\right) \int_{t'_{m-}}^{t'_m} \left(G^d + G^c\right) dt\, dt' \\
& + (\hat{n}'_{n-} \cdot \hat{t}_m) \int_{t'_{n-1}}^{t'_n} \left(1 - \frac{t'_n - t'}{\Delta_{n-1}}\right) \int_{t'_m}^{t'_{m+}} \left(G^d + G^c\right) dt\, dt' \\
& + (\hat{n}'_n \cdot \hat{t}_{m-}) \int_{t'_n}^{t'_{n+1}} \left(1 - \frac{t' - t'_n}{\Delta_n}\right) \int_{t'_{m-}}^{t'_m} \left(G^d + G^c\right) dt\, dt' \\
& + (\hat{n}'_n \cdot \hat{t}_m) \int_{t'_n}^{t'_{n+1}} \left(1 - \frac{t' - t'_n}{\Delta_n}\right) \int_{t'_m}^{t'_{m+}} \left(G^d + G^c\right) dt\, dt' \Bigg\}
\end{aligned}
\tag{C.21}
$$

where the following dot product notation has been adopted: the subscripts n_ and m_ refer to unit vectors at segment locations $\Delta\ell_{n-1}$ and $\Delta\ell_{m-1}$, respectively; the subscripts n and m

refer to the unit vectors located at segments $\Delta\ell_n$ and $\Delta\ell_m$, respectively. To numerically evaluate (C.21) in its present form requires four double integrations — a very time consuming process. To remedy this problem, we approximate the inner integral. Specifically, we make the course approximation that the integrand is relatively constant over the interval of integration. This "constant" value is taken to be the integrand evaluated at the midpoint of the the limits of integration. When the source point and field point are in the same segment (called the self-patch segment), the integrand varies dramatically (in fact, the Hankel has a singularity in this segment). However, since the dot product term is zero, our assumption is not invalidated. The approximate form of (C.21) becomes

$$
\begin{aligned}
-jk_z \sum_{n=1}^{N} M_n^t \Bigg\{ & (\hat{n}'_{n-} \cdot \hat{t}_{m-}) \int_{t'_{n-1}}^{t'_n} \left(1 - \frac{t'_n - t'}{\Delta_{n-1}}\right) \frac{\Delta_{m-1}}{4} \left(G^d + G^c\right)_{m-/2} \, dt' \\
& + (\hat{n}'_{n-} \cdot \hat{t}_m) \int_{t'_{n-1}}^{t'_n} \left(1 - \frac{t'_n - t'}{\Delta_{n-1}}\right) \frac{\Delta_m}{4} \left(G^d + G^c\right)_{m+/2} \, dt' \\
& + (\hat{n}'_n \cdot \hat{t}_{m-}) \int_{t'_n}^{t'_{n+1}} \left(1 - \frac{t' - t'_n}{\Delta_n}\right) \frac{\Delta_{m-1}}{4} \left(G^d + G^c\right)_{m-/2} \, dt' \\
& + (\hat{n}'_n \cdot \hat{t}_m) \int_{t'_n}^{t'_{n+1}} \left(1 - \frac{t' - t'_n}{\Delta_n}\right) \frac{\Delta_m}{4} \left(G^d + G^c\right)_{m+/2} \, dt' \Bigg\}
\end{aligned}
\tag{C.22}
$$

where $m+/2$ (or $m-/2$) reminds us that the observation point is to located at midway between the points t'_m and t'_{m+} (or midway between t'_{m-} and t'_m). If we let $\mathbb{D}^d_{mn} + \mathbb{D}^c_{mn}$ represent the terms inside the bracket, then (C.22) may be written as

$$
-jk_z \sum_{n=1}^{N} M_n^t \left(\mathbb{D}^d_{mn} + \mathbb{D}^c_{mn}\right) \quad . \tag{C.23}
$$

The last term of (C.18) has the same form as the first term. If we follow the above procedure and make the same approximations, this term may be written as

$$
\sum_{n=1}^{N} J_n^t \left(\frac{k_d^{\,2}}{j\omega\epsilon_d^*} \mathbb{H}^d_{mn} + \frac{k_c^{\,2}}{j\omega\epsilon_c^*} \mathbb{H}^c_{mn} \right) \tag{C.24}
$$

where

$$H^{d}_{mn} \equiv (\hat{t}'_{n-} \cdot \hat{t}_{m-}) \int_{t'_{n-1}}^{t'_n} \left(1 - \frac{t'_n - t'}{\Delta_{n-1}}\right) \frac{\Delta_{m-1}}{4} \left(G^{d}\right)_{m-/2} \, dt'$$

$$+ (\hat{t}'_{n-} \cdot \hat{t}_{m}) \int_{t'_{n-1}}^{t'_n} \left(1 - \frac{t'_n - t'}{\Delta_{n-1}}\right) \frac{\Delta_{m}}{4} \left(G^{d}\right)_{m+/2} \, dt'$$

$$+ (\hat{t}'_{n} \cdot \hat{t}_{m-}) \int_{t'_{n}}^{t'_{n+1}} \left(1 - \frac{t' - t'_n}{\Delta_{n}}\right) \frac{\Delta_{m-1}}{4} \left(G^{d}\right)_{m-/2} \, dt'$$

$$+ (\hat{t}'_{n} \cdot \hat{t}_{m}) \int_{t'_{n}}^{t'_{n+1}} \left(1 - \frac{t' - t'_n}{\Delta_{n}}\right) \frac{\Delta_{m}}{4} \left(G^{d}\right)_{m+/2} \, dt' \, . \qquad \text{(C.25)}$$

The definition for H^{c}_{mn} is the same as (C.25) with G^{c} substituted for G^{d}.

The second term of (C.18) is equivalent to

$$\sum_{n=1}^{N} M^{z}_{n} \left\{ \int_{t'_{m-}}^{t'_m} \int_{t'_n}^{t'_{n+1}} \left(\frac{\partial G^{d}}{\partial n} + \frac{\partial G^{c}}{\partial n} \right) dt' \, dt \right.$$

$$\left. + \int_{t'_m}^{t'_{m+}} \int_{t'_n}^{t'_{n+1}} \left(\frac{\partial G^{d}}{\partial n} + \frac{\partial G^{c}}{\partial n} \right) dt' \, dt \right\} \, . \qquad \text{(C.26)}$$

To reduce (C.26) to a single integral, we first reverse the order of integration and assume the integrand is constant over the interval of integration. Again, we take the "constant" value to be the integrand evaluated at the midpoint of the limits. This process gives

$$\sum_{n=1}^{N} M^{z}_{n} \left\{ \int_{t'_n}^{t'_{n+1}} \left(\frac{\partial G^{d}}{\partial n} + \frac{\partial G^{c}}{\partial n} \right)_{m-/2} dt' \right.$$

$$\left. + \int_{t'_n}^{t'_{n+1}} \left(\frac{\partial G^{d}}{\partial n} + \frac{\partial G^{c}}{\partial n} \right)_{m+/2} dt' \right\} \qquad \text{(C.27)}$$

where the notation has been defined in (C.22). From (C.5) we have

$$\frac{\partial G^{d}}{\partial n} = \frac{k^{d}_{\rho}}{j4} \cos\alpha \, H^{(2)}_{1}\left(k^{d}_{\rho} \, |\rho - \rho'|\right) \qquad \text{(C.28)}$$

where α is the angle between $\hat{\mathbf{n}}$ and the vector from the observation point to the source point $(\rho' - \rho)$ — see Fig. C.1. Using the previous notation (see C.7), we have

$$\frac{\partial G^d}{\partial n} = -\frac{k_\rho^d}{j4}\left(\hat{\mathbf{R}}\cdot\hat{\mathbf{n}}\right) H_1^{(2)}\left(k_\rho^d\ |\rho-\rho'|\right) \quad . \tag{C.29}$$

The first order Hankel function exhibits a singularity in the self-patch segment. Again, the singularity is nullified by a dot product (see C.29). We define the bracketed terms in (C.27) as $\mathbb{E}^d_{mn} + \mathbb{E}^c_{mn}$ giving

$$\sum_{n=1}^{N} M_n^z\left(\mathbf{E}^d_{mn} + \mathbf{E}^c_{mn}\right) \ . \tag{C.30}$$

The third term in (C.18) has the form

$$\sum_{n=1}^{N} J_n^t \int_{t'_{m-}}^{t'_{m+}} \frac{\partial}{\partial t} \int_{t'_{n-1}}^{t'_{n+1}} \left(\frac{G^d}{j\omega\epsilon_d^*} + \frac{G^c}{j\omega\epsilon_c^*}\right) \frac{\partial}{\partial t'}\left(1 - \frac{|t'-t'_n|}{\Delta}\right) dt'\, dt \tag{C.31}$$

Once the inner integral of (C.31) is calculated, we are left with a function of t. For convenience, let this function be defined as $f(t)$. Next, $f(t)$ is differentiated and then integrated from t'_{m-} to t'_{m+} The above operations are equivalent to finding $f(t'_{m-}) - f(t'_{m+})$. Thus, (C.31) becomes,

$$\sum_{n=1}^{N} J_n^t \int_{t'_{n-1}}^{t'_{n+1}} \frac{\partial}{\partial t'}\left(1 - \frac{|t'-t'_n|}{\Delta}\right)\left(\frac{1}{j\omega\epsilon_d^*}\left[(G^d)_{m+} - (G^d)_{m-}\right]\right.$$

$$\left. + \frac{1}{j\omega\epsilon_c^*}\left[(G^c)_{m+} - (G^c)_{m-}\right]\right) dt' \tag{C.33}$$

where the notation $m+$ (or $m-$) signifies that the observation point is to be located at t'_{m+}

(or t'_{m+}). Carrying out the derivatives yields,

$$\sum_{n=1}^{N} J_n^t \left\{ \frac{1}{j\omega\epsilon_d^*} \left(\int_{t'_{n-1}}^{t'_n} \frac{1}{\Delta_{n-1}} \left[(G^d)_{m+} - (G^d)_{m-} \right] dt' \right. \right.$$

$$\left. - \int_{t'_n}^{t'_{n+1}} \frac{1}{\Delta_n} \left[(G^d)_{m+} - (G^d)_{m-} \right] dt' \right)$$

$$+ \frac{1}{j\omega\epsilon_c^*} \left(\int_{t'_{n-1}}^{t'_n} \frac{1}{\Delta_{n-1}} \left[(G^c)_{m+} - (G^c)_{m-} \right] dt' \right.$$

$$\left. \left. - \int_{t'_n}^{t'_{n+1}} \frac{1}{\Delta_n} \left[(G^c)_{m+} - (G^c)_{m-} \right] dt' \right) \right\} . \qquad \text{(C.34)}$$

We define the first two integrals in (C.34) as F^d_{mn} , and the remaining two are defined as F^c_{mn}. Now, (C.34) may be written as

$$\sum_{n=1}^{N} J_n^t \left(\frac{1}{j\omega\epsilon_d^*} F^d_{mn} + \frac{1}{j\omega\epsilon_c^*} F^c_{mn} \right) \qquad \text{(C.35)}$$

The fourth term in (C.18) is equivalent to

$$-jk_z \sum_{n=1}^{N} J_n^z \int_{t'_{m-}}^{t'_{m+}} \frac{\partial}{\partial t} \int_{t'_n}^{t'_{n+1}} \left(\frac{1}{j\omega\epsilon_d^*} G^d + \frac{1}{j\omega\epsilon_c^*} G^c \right) dt' \, dt \ . \qquad \text{(C.36)}$$

Following the same steps as above,

$$-jk_z \sum_{n=1}^{N} J_n^z \left(\frac{1}{j\omega\epsilon_d^*} \int_{t'_n}^{t'_{n+1}} \left((G^d)_{m+} - (G^d)_{m-} \right) dt' \right.$$

$$\left. + \frac{1}{j\omega\epsilon_c^*} \int_{t'_n}^{t'_{n+1}} \left((G^c)_{m+} - (G^c)_{m-} \right) dt' \right) . \qquad \text{(C.37)}$$

If we define G^d_{mn} as the first integral in (C.37) and G^c_{mn} as the second, then (C.37) can be written as

$$-jk_z \sum_{n=1}^{N} J^z_n \left(\frac{1}{j\omega\epsilon^*_d} G^d_{mn} + \frac{1}{j\omega\epsilon^*_c} G^c_{mn} \right) . \tag{C.38}$$

Using (C.23), (C.24), (C.30), (C.35), and (C.38), equation (C.18) may be written as

$$\begin{aligned} &-jk_z \sum_{n=1}^{N} M^t_n \left(D^d_{mn} + D^c_{mn} \right) + \sum_{n=1}^{N} M^z_n \left(E^d_{mn} + E^c_{mn} \right) \\ &\quad + \sum_{n=1}^{N} J^t_n \left(\frac{1}{j\omega\epsilon^*_d} F^d_{mn} + \frac{1}{j\omega\epsilon^*_c} F^c_{mn} \right) \\ &\quad - jk_z \sum_{n=1}^{N} J^z_n \left(\frac{1}{j\omega\epsilon^*_d} G^d_{mn} + \frac{1}{j\omega\epsilon^*_c} G^c_{mn} \right) \\ &\quad + \sum_{n=1}^{N} J^t_n \left(\frac{k_d^2}{j\omega\epsilon^*_d} H^d_{mn} + \frac{k_c^2}{j\omega\epsilon^*_c} H^c_{mn} \right) = 0 \ , \ m = [1 \ldots N] \ . \end{aligned} \tag{C.39}$$

The vita has been removed from the scanned document